# A high-resolution elemental record of post-glacial lithic sedimentation in Upernavik Trough, western Greenland: History of ice-sheet dynamics and ocean circulation changes over the last 9100 years

Jacques Giraudeau, E. Georgiadis, M. Caron, P. Martinez, G. Saint-Onge, I. Billy, P. Lebleu, O. Ther, Guillaume Massé

# A high-resolution elemental record of post-glacial lithic sedimentation in Upernavik Trough, western Greenland: history of ice-sheet dynamics and ocean circulation changes over the last 9 100 years.

**J. Giraudeau[1], E. Georgiadis[1,2], M. Caron[3], P. Martinez[1], G. Saint-Onge[3], I. Billy[1], P. Lebleu[1], O. Ther[1], and G. Massé[2,4]**

[1]Université de Bordeaux, CNRS, UMR 5805 EPOC, 33615 Pessac, France

[2]Université Laval, CNRS, UMI 3376 TAKUVIK, Québec, G1V 0A6, Canada

[3]Université du Québec à Rimouski and GEOTOP Research Center, Institut des sciences de la mer de Rimouski (ISMER), Rimouski, G5L 3 A1, Canada

[4]Université Paris VI, CNRS, UMR 7159 LOCEAN, 75005 Paris, France

Corresponding author: Jacques Giraudeau (jacques.giraudeau@u-bordeaux.fr)

## Abstract

A better understanding of the past dynamics of local sectors of the Greenland ice sheet (GIS) with regards to ocean circulation and climate changes can be developed from proxy records derived from marine sedimentary archives. Here we investigate the post 9.1 cal. kyr BP history of the western sector of the GIS from the XRF core scanner-derived geochemistry of a sediment core retrieved from Upernavik Trough, Melville Bay. The elemental signature of material derived from Melville Bay glaciers, Upernavik Isstrom and Rink Isbrae can be inferred from the geology of the bedrocks drained by these major ice streams of the western GIS. Changes in abundance of Fe-rich basaltic material reflect changes in West Greenland Current (WGC) strength. Contributions from Melville Bay glaciers were dominant during the early part of the record as a result of the rapid retreat of this stretch of the NW GIS. Atmospheric warming and strengthened WGC between 7.5 and 5 cal. kyrs BP promoted contributions from distal southern sources of lithic material to the sedimentation over Upernavik Trough. The Neoglacial shift in climate and ocean circulation led to a general reduction in the delivery of lithic material from western GIS glacier outlets glaciers. The particular geomorphology of the fjord hosting Rink Isbrae as well as the important depth of the Uummannaq Trough likely explain the high relative contribution of this glacier to the lithic sedimentation over Upernavik Trough during the later part of the Holocene despite a weakened WGC.

## Keywords

West Greenland; Holocene; tidewater glaciers; climate changes; ocean circulation

## 1 Introduction

Compared to other sectors of the Greenland Ice Sheet (GIS), western and northwestern Greenland from 69°N to 76°N mainly hosts fast moving glaciers with speeds commonly exceeding 3 km/yr (Rignot and Mouginot, 2012; MacGregor et al., 2016). This spatial heterogeneity in ice flow speed illustrates the role on ice sheet dynamics of marine terminating glaciers which drain most of west and northwest Greenland. The cumulative drainage area of western and northwestern glaciers is in the order of 460 000 km² and represents 30% of the total GIS surface (Rignot and Mouginot, 2012). The northward transport of warm Atlantic Water (AW) carried by the West Greenland Current (WGC) in eastern Baffin Bay and its role on the direct melting of major tidewater glacier termini as well as on regional atmospheric temperatures and precipitations explain most of the modern changes in ice flow and mass loss of outlet glaciers in this sector (Chauché et al., 2014; Sakakibara and Sugiyama, 2018). Marine geological studies of sediment cores collected over the slope and within cross-shelf troughs off western Greenland have demonstrated that ocean warming linked to the initiation of the WGC ca. 15 cal. kyrs BP was pivotal in driving, together with the orbitally-induced increase in boreal summer temperature, the retreat of the grounded GIS from the shelf edge to its near-modern position during the last deglaciation (Sheldon et al., 2016; Jennings et al., 2017; Jennings et al., 2018). This ocean – ice-sheet connection is seen as a persistent feature explaining mid to late Holocene glacier changes (advances, retreats) in local sectors of central West Greenland (Schweinsberg et al., 2017). Both ice-sheet model simulations (Lecavalier et al., 2014) and $^{10}$Be and $^{14}$C dating of ice-marginal systems (Young and Briner, 2015; Sinclair et al., 2016; and references therein) suggest that the GIS retreat from the west Greenland shelf (WGS) was completed by ca. 10 cal. kyrs BP. This extensive deglacial retreat of the western GIS was accompanied by a massive delivery of terrigenous material to the shelf and slope *via* iceberg

calving, meltwater plumes and sediment gravity flows. These reached the shelf edge through a series of bathymetric troughs interpreted as paleo ice-streams (Fig. 1), namely from south to north Disko Trough, Uummannaq Trough, Upernavik Trough, and Melville Bay (Ó Cofaigh et al., 2013; Hogan et al., 2016; Sheldon et al., 2016; Newton et al., 2017). Following the last deglaciation, sedimentation over the WGS is assumed to derive mainly from iceberg rafting and sediment plumes from proximal and southerly sources and is subjected to subsequent redistribution under the influence of the northward flowing WGC (Andrews et al., 2018). Holocene changes in primary productivity and sedimentation of marine organic matter over the west Greenland shelf are intimately linked to sea ice dynamics. Sea ice and surface conditions in eastern Baffin Bay are mainly constrained by temperature and salinity variations of the WGC, which are themselves controlled by the changing contribution of Irminger water to this current and the variable input of freshwater from the bordering GIS (e.g. Myers et al., 2007). Baffin Bay ice cover is also controlled by the North Atlantic Oscillation (NAO) through its effect on regional atmospheric temperatures. Accordingly, cooler air temperature and greater sea ice extent in Baffin Bay generally occur during positive phase of the NAO (Wang et al., 1994; Stern and Heide-Jørgensen, 2003).

High resolution, continuous biotic proxy records obtained from marine sediment cores off western Greenland, especially in the Disko Bay region, have been widely used in the past 10-15 years to shed light on the intricate connection between hydrographic conditions and the behavior of the western GIS over the Holocene (Lloyd et al., 2005 and 2007; Moros et al., 2006; Perner et al. 2012 and 2013; Sha et al., 2014; Krawczyk et al., 2016; among others). More recently, mineralogy has been used to assess the provenance of sediment from the various ice-sheets draining into Baffin Bay over the last glacial cycle (Andrews et al., 2012; Simon et al., 2014) by applying a sediment-unmixing program to the bulk mineralogy of marine sediments and taking into account the bedrock

geology underlying major ice-streams (Andrews and Eberl, 2011). This methodological approach was pivotal in distinguishing eastern (Greenland), northern (Ellesmere Isl.), and western (Baffin Isl.) contributions to the late Pleistocene sedimentation in Baffin Bay, and hence to discuss the synchroneity in the behaviors of the ice-sheets which drained these regions (Andrews et al., 2018; and references therein).

A thorough compilation of chemical analyses of stream sediment samples undertaken by the Geological Survey of Denmark and Greenland (Steenfelt, 2001) showed that the distribution patterns of many major and trace elements closely reflects the various rock complexes of western Greenland, and discriminates local bedrock formations drained by distinct, major marine terminating glaciers between 68°N and 73°N. The present study investigates the geochemical (elemental) composition of a marine sediment core collected over the shelf of western Greenland in order to track potential changes in the delivery of local and distal glacial sources over the last 9100 years. The reconstructed continuous, high resolution patterns in lithogenic provenance might unravel distinct post-glacial behaviors of major marine-terminating glaciers of western Greenland, as well as Holocene changes in the strength of the main process (WGC) of transport and redistribution of lithic material over the west Greenland shelf.

## 2 Environmental and geological setting

The main features of the onshore geology of western Greenland as well as the hydrography and bathymetry of the adjoining shelf are summarized in Figure 1. We restricted this short summary to the region extending from ca. 68°N to 75°N which includes some of the main proximal and distal glacial tributaries which are thought to contribute to the lithic sedimentation at the studied core location (Upernavik Trough).

The bedrock of western Greenland varies in age from Archaean to Paleogene (Escher and Pulvertaft, 1995). According to Steenfelt et al. (1998) and the 1:250 000 geological map of Henriksen et al. (2000), the exposed bedrock belongs to 4 main geological formations (Fig. 1):

- Reworked Archean gneisses in the southern sector of Uummannaq Bay and in Disko Bay which are essentially drained by Store Gletscher and Jakobshavn Isbrae respectively, with rare felsic intrusions and small lenses of unspecified supracrustal rocks;
- Palaeoproterozoic metasediments (schists) belonging to the Karrat Group in the northern sector of Uummannaq Bay drained by Rink Isbrae, as well as north of 73°N where maximal GIS extent strongly limits surface exposure;
- A felsic Paleoproterozoic intrusion (Prøven granite) across the Karrat Group formation, which is essentially drained by Upernavik Isstrom and its tributaries;
- Tertiary (Lower Paleogene) basalts distributed within the western sectors of Disko Bay (over Disko Island) and Uummannaq Bay. Draining of this intrusive formation by the GIS is limited, being restricted to the northernmost basaltic flows immediately south of the Prøven granite.

The ocean circulation over the WGS is controlled by the northward flowing WGC. Water masses carried by the WGC reach the calving fronts of major tidewater glaciers in Disko, Uummannak and Melville bays through cross-shelf glacial troughs and deep-silled fjords and therefore influences their dynamics (Chauché et al., 2014). Previous studies, such as those conducted in Melville Bay on Upernavik Isstrom (Fig. 1) and its associated fjord (Upernavik Isfjord) (Weidick, 1958; Andresen et al., 2014) highlighted the importance of fjord bathymetry on the dynamics of outlet glaciers, as well as the impact of WGC warming episodes on their recent ($20^{th}$ century) retreat episodes. The main and secondary branches of the WGC redistribute glacier and stream-derived material as well as sediment eroded from exposed coastal formations in a northward

direction over the mid to outer shelf (Fig. 1). The WGC is also responsible for the near zonal distribution of sea ice in Baffin Bay: according to the opposing flow of Arctic- and Atlantic-derived water masses on the western and eastern sides of Baffin Bay, respectively, sea ice extent follows a southwest-northeast trend shifting from north to south from September to March. The study area presently hosts the southernmost limit of maximum winter sea ice concentrations (>90%) in eastern Baffin Bay within the northern sector of Uummannaq Bay (Fig. 1; Stern and Heide-Jorgensen, 2003). The physiography and hydrography of Upernavik trough where the marine sediment core studied in this paper has been collected, has been described by Andresen et al. (2014).

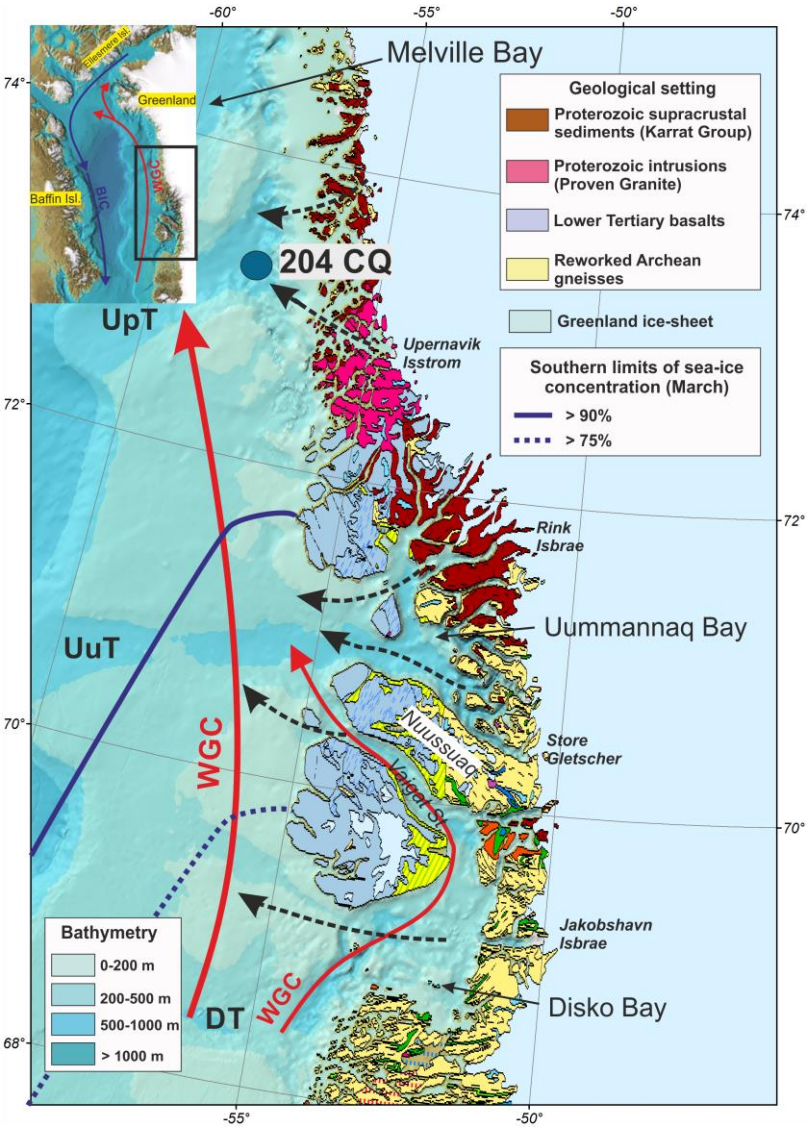


Figure 1: Main elements of the bedrock geology of western Greenland (after Henriksen et al., 2000) and of the hydrology on the nearby shelf. Black dotted arrows highlight the delivery of glacial material to the shelf from the fastest moving glaciers in the area as well as from the Melville Bay sector of the GIS (according to Rignot and Mouginot, 2012). Mean sea ice concentrations refers to the month (March) of maximum sea ice extent in Baffin Bay (after NSDIC climatological maps, and Stern and Heide-Jorgensen, 2003). WGC: West Greenland Current. BIC: Baffin Island Current. UpT: Upernavik Trough; UuT: Uummannaq Trough; DT: Disko Trough. Blue dot: location of the studied core 204 CQ. The inserted map (upper left corner) shows the regional oceanography and wider setting of the studied area.

## 3 Material and Methods

The 734-cm long giant, square, gravity core AMD 204 CQ (hereafter referred to as 204 CQ) studied here was collected at the head of Upernavik Trough (73°15.66'N, 57°53.98'W, 987 m. water depth) as part of the 2014 ArcticNet expedition of the CCGS *Amundsen*. The core was

immediately sampled onboard using large U-channels. The lithology is homogeneous and consists of bioturbated clayey silts (Caron et al., 2018).

### 3.1 Sedimentological analyses

High-resolution images were routinely acquired on the whole U-channels using a computed tomography (CT) scanner (Siemens SOMATOM Definition AS+128 at the Institut National de la Recherche Scientifique, Quebec, Canada) which records down-core changes in bulk density from variations in the CT-numbers (Fortin et al., 2013). The images were also used to locate mollusk shell-rich areas for subsequent $^{14}C$ dating, and to check for the presence of lithofacies which might have been missed during visual examination. Grain-size analyses were performed on bulk sediment every 8 cm using a Beckman Coulter LS13320 laser diffraction grain-size analyzer (0.04-2000 µm) and results are expressed as % particles of the various size fractions ranging from clay to very coarse sand. Full details of CT scan and grain size analyses conducted on core 204 CQ are shown in Caron et al. (2018).

### 3.2 XRF core scanning

Downcore X-ray fluorescence (XRF) scanning was conducted on core 204 CQ at 0.5 cm resolution using an AVAATECH core scanner with generator settings of 10, 30 and 50 kV to record net intensities of 18 elements ranging from Al to Ba (Table 1). Raw XRF data were normalized to the sum of all element intensities, then log transformed, in order to correct for changes induced by down-core variations in grain size, water content and surface roughness (Bouchard et al., 2011; Martin et al., 2014; Baumann et al., 2017). For simplification, all log-transformed ratios data will be referred to by the symbol of the normalized element in the following text and figures.

The database of element (ppm) or oxide (%) concentrations measured in stream sediment samples from western Greenland (Steenfelt, 2001; and Greenland portal of www.greenmin.gl) was

extracted to illustrate the concentration ranges, within each of the above-described geological provinces, of the 18 elements measured in the present study by the XRF core scanner (Table 1).

| | Karrat North (412) | Prøven granite (501) | Tertiary basalts (542) | Karrat South (1010) | Archean gneisses (1274) |
|---|---|---|---|---|---|
| Al2O3 (%) | 13->23 (16) | 13-15 (14.5) | <13.6 (12.3) | 13-15 (14) | 13-16 (14.4) |
| *SiO2 (%)* | *50-70 (66)* | *50-70 (63)* | *< 60 (49)* | *50-70 (65)* | *50-70 (65)* |
| TiO2 (%) | 0.4-0.7 (0.6) | ~ 1.5 | 1.5->4.5 (2.2) | 0.7-2 (0.8) | <0.5 |
| Fe2O3 (%) | 5.1-10.6 (7) | 5.1-8.7 (8) | **13.1-18.6 (15)** | 5.6-10.6 (9) | 3.2-6.1 (4.3) |
| MnO (%) | 0.05-0.1 (0.07) | 0.07-0.15 (0.1) | 0.18-0.26 (0.2) | 0.06-0.18 (0.1) | 0.05-0.09 (0.07) |
| *CaO (%)* | *<1.9 (1.8)* | *<1.9 (1.8)* | *1.1-11.8 (9.4)* | *<1.9 (1.5)* | *2.6-4.6 (3.6)* |
| K2O (%) | **3.1-3.8 (3.2)** | **3.1-4.2 (3.5)** | <0.8 (0.3) | 1.9-2.6 (2.4) | 1.5-2.6 (2) |
| *Ba (ppm)* | *450-660 (580)* | *740-1020 (910)* | *<290 (96)* | *510-660 (564)* | *400-740 (575)* |
| *Br (ppm)* | *2-84 (27)* | *15-40 (16)* | *<2-18 (3)* | *<2* | *8-120 (16)* |
| Cr (ppm) | 60->2900 (89) | 20-75 (66) | 330->2900 (1140) | 110-660 (180) | 20-90 (85) |
| Ni (ppm) | <15-79 (37) | <15-41 (27) | 79->630 (285) | 79->630 (131) | <15-79 (35) |
| Rb (ppm) | 109-142 (128) | 125->142 (105) | <20 (4) | 66-109 (90) | 30-109 (52) |
| *Sr (ppm)* | *<218 (166)* | *175-312 (250)* | *140-218 (173)* | *<164 (157)* | *175-380 (305)* |
| Zn (ppm) | 48-127 (74) | 80-152 (113) | 70-127 (94) | **127->620 (213)** | <32-70 (40) |
| Zr (ppm) | 310-690 (434) | **690-1200 (950)** | Below detection limits | Below detection limits | 180-690 (344) |

Table 1: Ranges and mean values (between brackets) of element and oxide concentrations within each of the main geological provinces of western Greenland from 75°N to 68°N according to the geochemical database (Greenland portal: www.greenmin.gl) compiled by Steenfelt (2001). The number of stream samples used for this compilation and which are representative of the various geological provinces, is given between brackets within the first line. The selected elemental markers for bedrock formations and their concentration ranges and mean values are highlighted in bold and underlined. Grey shadings and italics: elements not considered in this study as unequivocal markers of bedrock formations in shelf sediments given their affinity to marine biogenic components of marine sediments.

These concentration ranges suggest that most bedrock formation can be tentatively characterized by peak values of elements of no equivalent concentration in another geological setting of the study area (Table 1). Hence, as a main constituent of ilmenite- and magnetite-rich basalts, Fe is enriched in material derived from these mafic rocks. As an original component of felsic intrusion, Zr is particularly concentrated in the restricted area of the Prøven granite drained by Upernavik Isstrom (Fig. 1). The northern and southern Karrat provinces can be differentiated by peak Zn concentrations in the later region drained by Rink Isbrae (Fig. 1 and Steenfelt et al., 1998).

Conversely, the northern Karrat formation hosts some of the highest K concentrations in stream sediments of the studied area together with the adjacent Prøven granite province. Finally, Archean gneisses in the southern Uummannaq and Disko Bay regions bear high concentrations of Sr (Table 1). This last element, as well as Si, Ca, Br, and Ba either show a clear affinity for marine organic matter export (Br, Ba), are main components of microfossil skeletons (Si and Ca), or are easily incorporated as trace elements into biogenic carbonates (Sr) (Calvert and Pedersen, 2007; and references therein). The unequivocal Sr signature of Archean bedrock-derived material in shelf sediments is therefore questionable and will not be discussed further in the present study.

Part of the dataset summarized in Table 1 was subjected to linear discriminant analyses (LDAs) in order to sustain the characterization of the different geological provinces by selected element and oxide concentrations. Separate LDAs were applied on datasets of element (Zr, Rb, Zn, Ni and Cr) and oxide ($Fe_2O_3$, $K_2O$, $TiO_2$ and $Al_2O_3$) concentration ranges with no affinity to marine biogenic components of marine sediments (Fig. 2, Table S1).

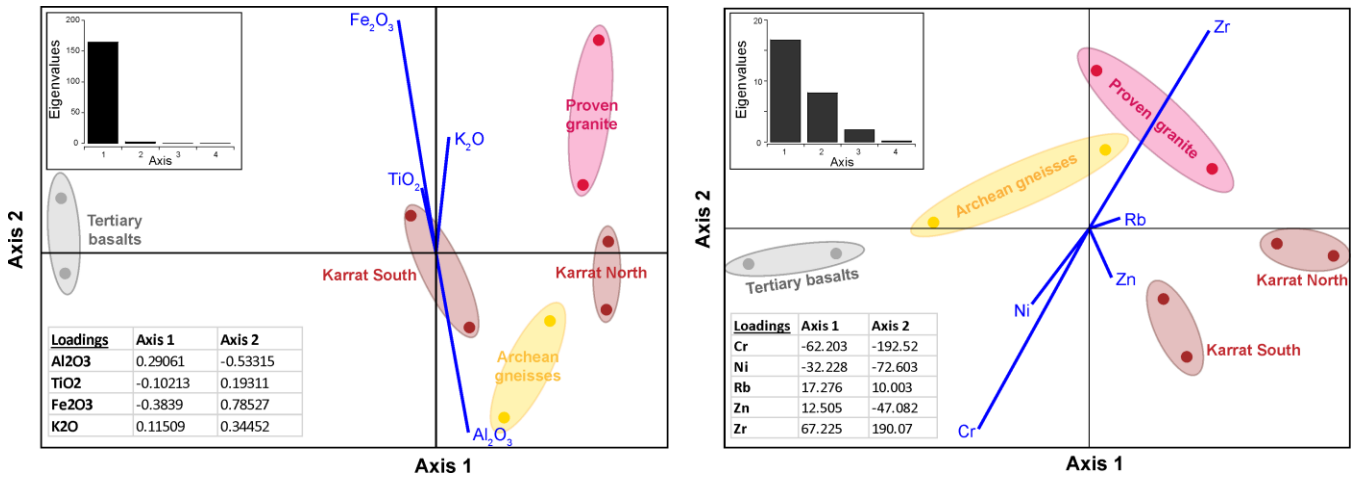


Figure 2: Summary plots of scores and loadings obtained after linear discriminant analyses of selected element (right plot) and oxide (left plot) concentration ranges within the five geological provinces of the studied area. The set of data used to construct these plots is given in Table S1.

When applied on oxide concentration ranges, LDA separates two groups of geological provinces along a single discriminant function (axis 1), the tertiary basalts (strong negative scores) vs. the northern Karrat, the Proven granite and the Archean gneiss provinces (positive scores). These two groups are explained by the opposite loadings of Fe (negative) and, $K_20$ and $Al_2O_3$ (both positive). Applying the same analysis on element concentration ranges essentially results into two discriminant functions (axes 1 and 2). According to loadings of the vertical axis 2, Zr (positive loadings) and Zn (negative loadings) are the main variables explaining the distribution of scores related to the elemental composition of rocks from the Proven granite and Karrat South, respectively. As suggested from the dataset of element and oxide concentration ranges (Table 1), and as confirmed by LDAs (Fig. 2), Archean bedrock-derived material cannot be characterized by typical element or oxide concentrations of no equivalent values in another geological setting of the study area. LDAs also confirm that Proven granite and northern Karrat rocks, which are both enriched in $K_2O$, can be differentiated by Zr content (high in Proven granites).

### 3.3 Age model of core 204 CQ

The age model used for core 204 CQ is an update of the one published by Caron et al. (2018) which was based on a combination of 4 AMS $^{14}C$ dates measured on benthic foraminifera (x4) and 12 paleomagnetic chronostratigraphic markers. Given the scarcity of benthic foraminifera in the top- and bottommost parts of core 204 CQ, and in order to improve the age model for these intervals, 10 additional AMS $^{14}C$ dates were measured on bulk organic matter. Table 2 and Fig. S1 show that organic matter $^{14}C$ dates are 2 to 3 000 years older on average than the ages expected from foraminiferal dates with a trend for higher differences with core depth. This inconsistency between biogenic carbonate and organic matter dates has been previously described as a common

feature of Deglacial and Holocene sediments in Baffin Bay and Labrador Sea sediments and has been attributed to significant influx of old carbon from reworked marine and/or terrestrial sediments following the Last Glacial Maximum (Andrews et al., 1985; Fillon et al., 1981; Licht et al., 1998).

The origin of the organic matter in core 204 CQ was assessed by measuring elemental (total organic carbon vs. total nitrogen (C/N)) and isotopic (delta $^{13}$C of organic matter ($\delta^{13}$Corg)) source identifiers downcore 204 CQ every ca. 10 cm. Total organic carbon content was measured on decarbonated (1N HCl) sediment using a LECO CS 125 analyzer (standard error of measurements < 0.5%). Total nitrogen and $\delta^{13}$Corg were measured simultaneously using a Carlo-Erba CN analyzer coupled to a Micromass-Isoprime mass spectrometer (analytical precision = 0.15‰). C/N and $\delta^{13}$Corg values (Fig. S1) range from 7 to 9.5 (mean = 8.1) and from 21.9‰ to 24.1‰ (mean = 23.0‰) (Fig. S1), respectively, indicating that the organic matter in core 204 CQ is essentially of marine origin (Meyers, 1994). The contribution of reworked terrestrial material to the organic matter in core 204 CQ is therefore minimal, *ie*. not detectable using standard elemental and isotopic source identifiers.

Following the method described by Andrews et al. (1985), we corrected the reported $^{14}$C dates measured on organic matter using an empirical equation [1] constructed from a comparison of the 4 uncalibrated $^{14}$C carbonate dates (*C*) obtained in core 204 CQ with projected organic matter dates (*O*) at the same core depth (Fig. S1, Table 2):

[1] $O = 1.237C + 1268$

All $^{14}$C dates were calibrated with the Calib 7.1 software (Stuiver et al., 2018) using the Marine09 calibration dataset and applying the local reservoir correction of 540 ($\Delta R = 140$) ± 35 years (Lloyd

et al., 2011). The final age-depth model (Fig. 3) was constructed with the R-package *Bacon* (Blaauw and Christen, 2011) which uses Bayesian statistics.

**14C dates**

| Lab number | Depth (cm) | Material dated | Delta 13C | Reported 14C age (yrs BP) | Reported error (±yrs BP) | Predicted 14C age after [1] (yrs BP) | Calibrated age (yrs BP) | 1 sigma | |
|---|---|---|---|---|---|---|---|---|---|
| | | | | | | | | from | to |
| BETA 480648 | 29-30 | Organic matter | -21.6 | 3290 | 30 | 1633 | 1044 | 973 | 1100 |
| BETA 480647 | 75-76 | Organic matter | -21.6 | 3780 | 30 | 2029 | 1437 | 1381 | 1499 |
| BETA 480646 | 125-126 | Organic matter | -21.8 | 4640 | 30 | 2724 | 2255 | 2196 | 2320 |
| BETA 480645 | 157-158 | Organic matter | -21.8 | 5650 | 30 | 3540 | 3268 | 3210 | 3333 |
| SacA 46004 | 169-171 | Mixed benthic & planktonic foraminifera | 5.7 | 3555 | 35 | | 3283 | 3222 | 3350 |
| BETA 480644 | 237-238 | Organic matter | -21.8 | 6410 | 30 | 4154 | 4026 | 3952 | 4096 |
| BETA 467785 | 251-253 | Mixed benthic & planktonic foraminifera | 0.3 | 4300 | 30 | | 4237 | 4149 | 4308 |
| BETA 480643 | 329-330 | Organic matter | -21.9 | 7820 | 30 | 5293 | 5517 | 5473 | 5568 |
| BETA 480642 | 491-492 | Organic matter | -22.5 | 8960 | 30 | 6214 | 6498 | 6430 | 6557 |
| BETA 488641 | 500-503 | Mixed benthic foraminifera | -1.8 | 6400 | 30 | | 6711 | 6652 | 6768 |
| SacA 46005 | 609-611 | Mixed benthic foraminifera & ostracods | -6.9 | 7445 | 50 | | 7767 | 7692 | 7831 |
| BETA 480641 | 613.5-614.5 | Organic matter | -22.9 | 10670 | 30 | 7596 | 7916 | 7864 | 7961 |
| BETA 480640 | 683-684 | Organic matter | -22.8 | 11170 | 30 | 8000 | 8328 | 8285 | 8379 |
| BETA 480639 | 713-714 | Organic matter | -22.8 | 11710 | 40 | 8436 | 8849 | 8770 | 8956 |

**Paleomagnetic chronostratigraphic markers**

| | Depth (cm) | Calibrated age (yrs BP) | Standard deviation |
|---|---|---|---|
| I1 | 58 | 1500 | 55 |
| I2 | 72 | 1675 | 119 |
| D1 | 75 | 1950 | 66 |
| P1 | 114 | 2325 | 137 |
| I3 | 115 | 2450 | 118 |
| P2 | 188 | 3375 | 199 |
| D2 | 198 | 3600 | 135 |
| P3 | 325 | 4875 | 239 |
| P4 | 367 | 5450 | 82 |
| I6 | 390 | 5925 | 103 |
| D3 | 460 | 6250 | 129 |
| P5 | 576 | 7200 | 122 |

Table 2: Radiocarbon dates (top) and paleomagnetic markers (bottom) used to construct the age-depth model of core 204 CQ. $^{14}C$ dates measured on calcareous material as well as paleomagnetic markers are taken from Caron et al. (2018). Reported $^{14}C$ dates measured on organic matter were corrected ("predicted $^{14}C$ ages") using an empirical equation ([1], Fig. S1) constructed from a comparison of the foraminiferal $^{14}C$ dates with projected organic matter $^{14}C$ dates at the same core depth.

According to the new age model, core 204 CQ covers a time interval from ca. 0.75 to 9.1 cal. kyrs BP. $^{210}Pb$ analyses showed no evidence of unsupported $^{210}Pb$ at the core-top (ie. older than ca. 100 years before 2014) hence confirming that core 204 CQ did not recover "modern" sediment (T. J. Andersen, Univ. Copenhagen; pers. comm.). Sedimentation rates average 0.1 cm/yr, peaking at 0.15 cm/yr around 6 cal. kyrs BP (Fig. 3).

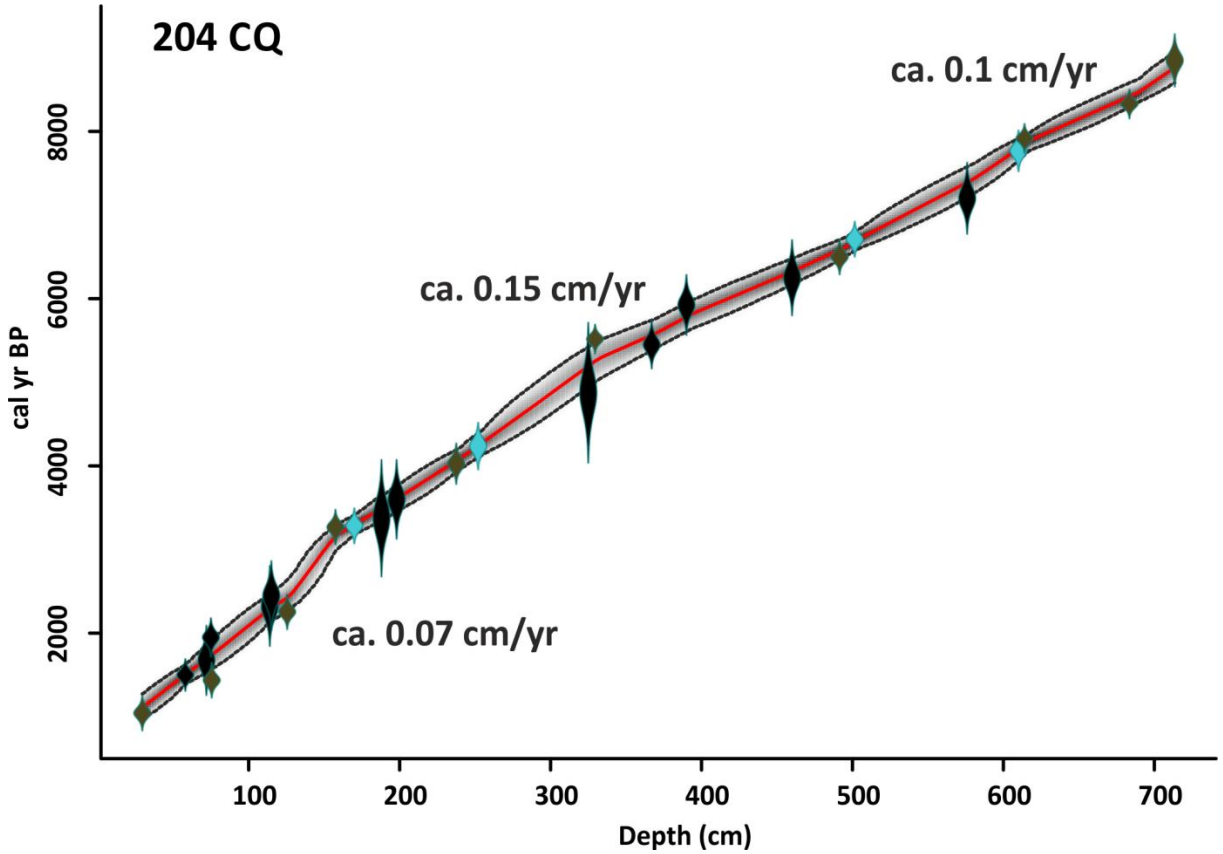


Figure 3: Age-depth model (revised from Caron et al., 2018) of core 204 CQ and mean sedimentation rates based on $^{14}C$ dates measured on foraminifera (blue diamonds) and organic matter (brown diamonds), and paleomagnetic stratigraphic markers (black diamonds). The black stippled lines bracket the 95% confidence intervals; the red curve shows the single 'best' model based on the mean age (Blaauw and Christen, 2011).

## 4 Results

### 4.1 Sedimentological data

Core 204 CQ consists of homogeneous bioturbated hemipelagic clayey silts with very rare and scattered occurrence of ice-rafted debris (IRD > 2 mm) (Caron et al., 2018). The sediment median grain size ($D_{50}$) which splits the distribution with half above and half below this diameter, ranges from ca. 3 to 6 µm and contains a short interval of dominantly silty clay centered at 6.8 cal. kyrs BP (Fig. 4). Highest grain sizes recorded in core 204 CQ fall within coarse and very coarse silts (31 – 63 µm) with a trend for higher values from ca. 7.2 cal. kyrs BP toward the core-top (Fig. 4). Smear slide analyses showed that this progressive coarsening might be partly induced by the increasing contribution of diatom skeletons to the sediment of core 204 CQ. The CT scan images do not provide any evidence of typical glacio-proximal facies such as laminated glacimarine deposits or coarse-grained subaqueous outwash deposits (Ó Cofaigh and Dowdeswell, 2001). This confirms that the location of core 204 CQ was in a distal position with regards to tidewater glacier termini of the GIS throughout the time interval covered by this sedimentary record, as expected from general reconstructions of the post-glacial dynamics of the western sector of the GIS (Lecavalier et al., 2014; Young and Briner, 2015). The absence of distinct IRD-rich horizons also suggests that catastrophic calving events of marine terminating glaciers along western Greenland, if any over the last ca. 9000 years, did not promote episodic, massive delivery of IRD to the core location.

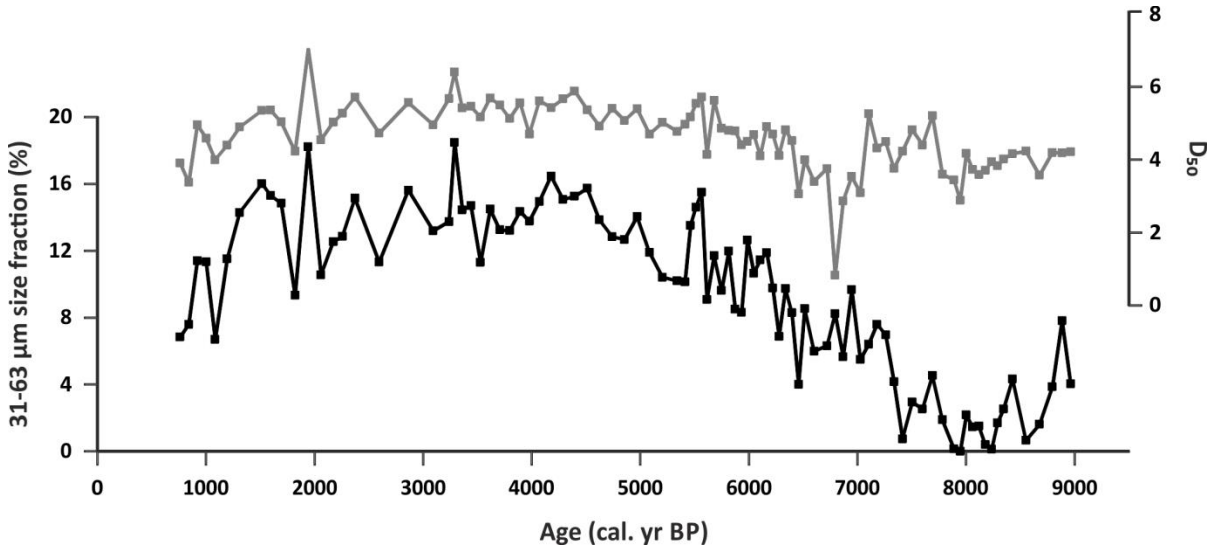


Figure 4: Median grain size ($D_{50}$ expressed in µm; full grey square) and contribution (%) of coarse and very coarse silts to the bulk sediment (full black square) in core 204 CQ.

## 4.2 XRF core scanning data

The down-core distribution of K, Zr, Fe and Zn intensities, as elemental markers of the Karrat North, Prøven granite, Lower Tertiary basalts, and Karrat South formations, respectively, is given in Figure 5. Those four elements display distinct long- and short-term patterns throughout core 204 CQ over the last 9000 years. K shows high values within the bottom part of the record from 9 to 7.5 cal. kyrs BP. Values thereafter decrease and remain rather low, though with two intervals of moderately higher intensities between ca. 5.5 and 3.5 cal. kyrs BP, and from 2 to 1 cal. kyrs BP. Zr shares with K a common long-term decrease in XRF intensity over the last ca. 9000 yrs. Millennial-scale changes are however opposite with broad peak Zr values occurring at the bottom-end of the core (ca. 9 cal. kyrs BP) as well as from 7.5 to 5.5 cal. kyrs BP. Outstanding, short-term, maximum Zr values are recorded at 8 and 6 cal. kyrs BP. Both the short events and the pattern of millennial-scale changes described for Zr are displayed by Zn. This last element however presents a long-term trend of increasing intensities from Early to Late Holocene, leading to a broad interval of maximum values between 3.5 and 2 cal. kyrs BP, as well as two additional short events of peak

intensities centered at 4.1 and 2.3 cal. kyrs BP. Finally the pattern displayed by Fe is intermediate to Zr and Zn, showing the same millennial scale variability but no long-term trend of decreasing or increasing values from ca. 7.5 cal. kyrs BP to the top of core 204 CQ. Maximum Fe intensities characterize a mid-Holocene interval from 7.5 to 5.5 cal. kyrs BP, as well as a single short event slightly after 6 cal. kyrs BP (ie. 5.8 cal. kyrs BP according to our age model).

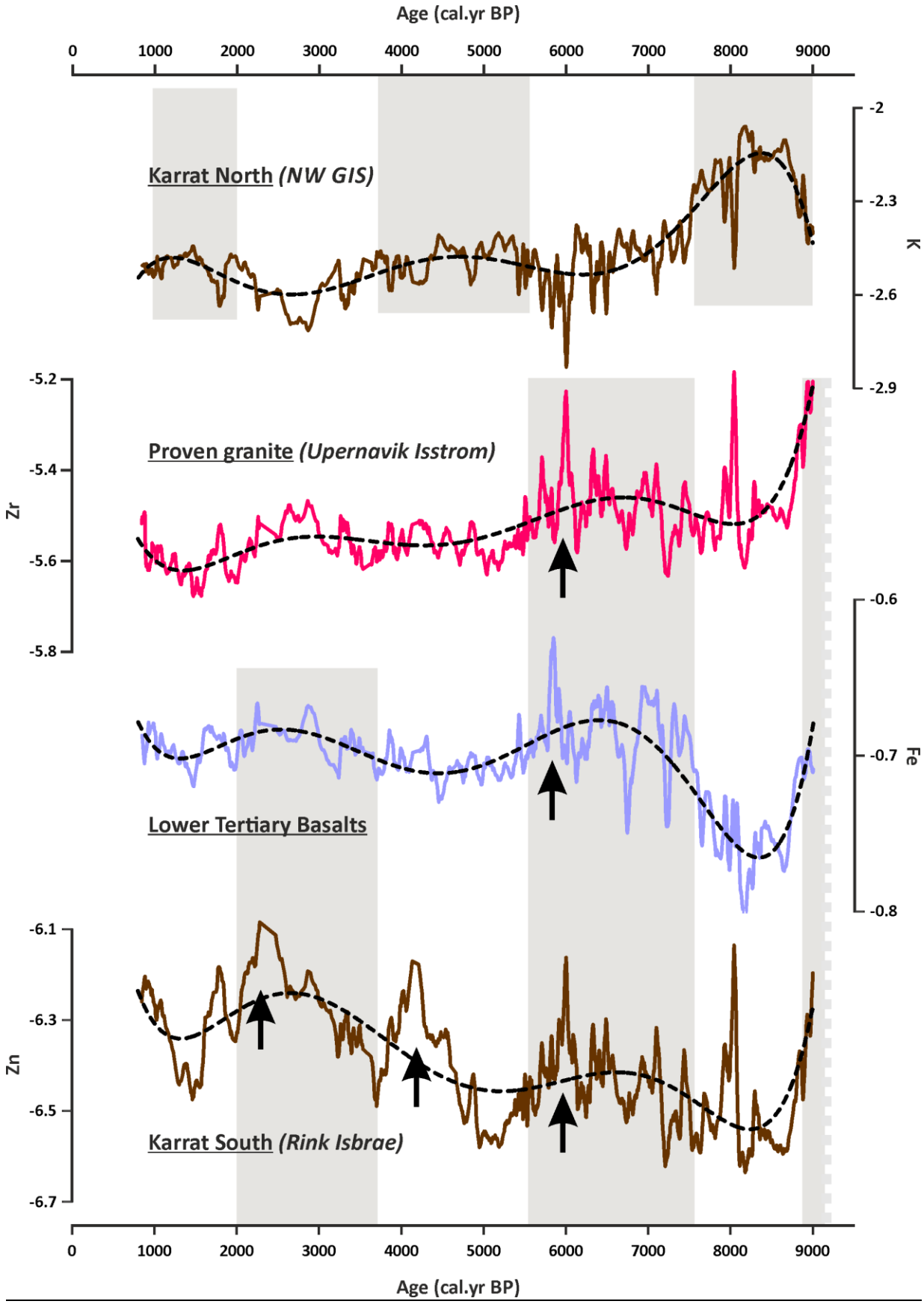
Age (cal.yr BP)
0
1000
2000
3000
4000
5000
6000
7000
8000
9000
Karrat North (NW GIS)
-2
-2.3
-2.6
-2.9
K
Proven granite (Upernavik Isstrom)
-5.2
-5.4
-5.6
-5.8
Zr
Lower Tertiary Basalts
-0.6
-0.7
-0.8
Fe
Karrat South (Rink Isbrae)
-6.1
-6.3
-6.5
-6.7
Zn
Age (cal.yr BP)

324

Figure 5: Patterns (10 point moving average) of XRF core scanner-derived elemental markers of bedrock sources in core 204 CQ: K, Zr, Fe and Zn, from top to bottom. Colors according to the mapped geological formations summarized in Figure 1. Names of major glaciers draining 3 or the 4 bedrocks are given in italics between brackets. Grey shaded areas highlight periods of sustained, high intensities of elemental markers according to a 6th order polynomial fitting curve (dashed black line). The vertical black arrows refer to remarkable events discussed in the text.

We applied principal component analysis (PCA) to identify the leading modes of variability among the whole set of XRF-derived element records. Results indicate that the first two principal components PC1 and PC2 account for 85% of total variance. PC1 (62% of the variance) is explained by two groups of positively and negatively correlated elements (Table 3 with inserted plot). High positive loadings to PC1 are expressed by Fe, Zn, and Ni which trace the distal southern basaltic (Fe and Ni) and Karrat South (Zn and Ni) sources of bedrock formations (Table 1); Br, S, and I whose concentrations in marine sediment are partly controlled by the production and subsequent burial of marine organic matter (Calvert and Pedersen, 2007), also show high positive loadings to PC1. Negative PC1 loadings are essentially expressed by K, the elemental marker for the Karrat North geological formation.

| | PC1 | PC2 |
|---|---|---|
| Al | **-0,889** | 0,400 |
| Si | **-0,817** | 0,541 |
| S | **0,931** | 0,094 |
| Cl | 0,771 | -0,586 |
| K | **-0,985** | 0,054 |
| Ca | -0,034 | **0,855** |
| Ti | -0,482 | **0,727** |
| Cr | 0,015 | 0,583 |
| Mn | -0,117 | -0,561 |
| Fe | **0,759** | -0,073 |
| Ni | **0,830** | -0,352 |
| Zn | **0,710** | -0,110 |
| Br | **0,910** | 0,327 |
| Rb | -0,349 | **-0,878** |
| Sr | **0,763** | -0,503 |
| Zr | 0,172 | **-0,832** |
| I | **0,856** | 0,471 |
| Ba | 0,275 | **-0,768** |

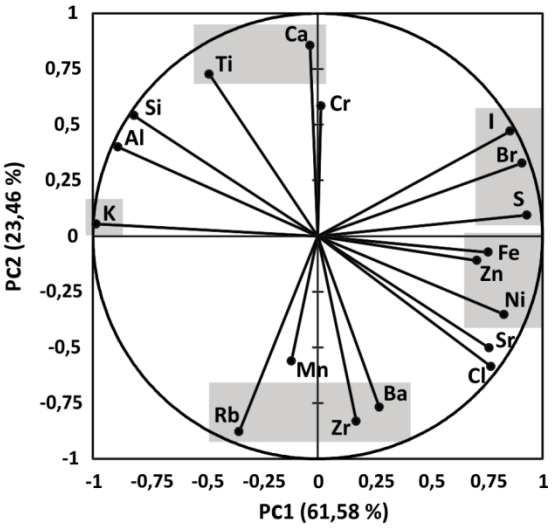

342 Table 3: Factor loadings on the first two principal component PC1 and PC2 for XRF core-scanning elemental data in
343 core 204 CQ. Inserted figure: distribution of loadings according to the first and second PC axes.
344

345 PC2, which explains 23% of the total variance, is (negatively) expressed by Zr and Rb and (though
346 with reduced loading) by Ba, those 3 elements being particularly concentrated in the Prøven granite
347 formation drained by Upernavik Isstrom (Table 1). High positive loading to PC2 is found for Ca,
348 an element which traces both marine biogenic (calcium carbonate) and lithogenic (basalts, see
349 Table 1) components of the marine sediments in the study area.
350 The PCA analysis statistically confirms the general patterns of variability described by the
351 elemental markers of specific bedrock formations shown in Figure 5:
352 - Changes in the relative contribution of Karrat North material in core 204 CQ over the last 9100
353 years are inversely related to relative contributions from distal basaltic and Karrat South
354 formations. The PCA grouping of these late distally-sourced elements (positive loadings in PC1)
355 presumably highlights the existence of a common transport vector (WGC) to the core location,
356 regardless of their mode of delivery to the shelf, ie. mainly glacial (Karrat South) vs. both glacial
357 and non-glacial - erosion of exposed coastal formations - (basalt formations).
358 - Holocene changes in the relative contribution of lithogenic material delivered from the proximal
359 Upernavik-draining Prøven granite bear a unique pattern (negative loadings in PC2), which
360 according to PCA orthogonal transformations, is linearly unrelated to the contributions of other
361 sources (explained by PC1).
362 Considering the undiscriminating information given by PC1 scores in terms of lithogenic sources
363 and erosional and transport processes (see above), as well as high loadings in both PC1 and PC2
364 of elements of known affinity with marine biogenic components, downcore records of PCA scores
365 can hardly be used in a straightforward manner to infer changes in provenance of lithogenic
366 material. We will therefore essentially refer hereafter to the XRF-derived profiles of the

normalized single elements (1) K, (2) Zr, (3) Fe, and (4) Zn as indicators of the variable contributions to the core location of material derived from (1) the southern Melville Bay sector of the GIS (Karrat North formation), (2) the Upernavik Isstrom which drains the Prøven granite formation, (3) the unglaciated coastal Lower Tertiary basalts, and (4) the Rink Isbrae and tributaries which drains the northern Uummannaq Bay sector of the GIS (Karrat South formation).

## 5 Discussion

The delivery of lithic material to the WGS is assumed to be essentially triggered by processes which are common to such high latitude settings: (1) ice loss from summer surface melting and runoff at the margin of the ice sheet, a process which is further accelerated in marine terminating glaciers under the influence of ocean melting of basal or frontal ice, and (2) the erosion of exposed (unglaciated) coastal formation as well as remobilization of shallow shelf sediment. Sea ice cover and duration might influence the transfer efficiency of lithic material to the ocean by prohibiting the export to the shelf of lithic-laden icebergs and land-fast ice from calving glaciers and the coastline, respectively. Subsequent transport by the WGC redistributes the lithic fraction delivered to the shelf or remobilized from shallow shelf deposits in a northward direction along the west Greenland margin. Modern (Chauché et al., 2014) and geological evidence (Thomas et al., 2016) also links strengthened transport of warm Atlantic Water (AW) carried by the WGC in eastern Baffin Bay to increases in regional atmospheric temperature and precipitation.

The observed changes in the relative contribution of K, Zr, Fe, and Zn in the sediments of core 204 CQ are therefore believed to be highly constrained by the local-scale responses of their source geological provinces and associated glacier dynamics to both climate and ocean forcing over the last 9100 years as well as by variations in strength of the along-shelf transport vector to the core

location. According to the distinct long and short term patterns displayed by the selected elements (Fig. 5), we suspect that the various source provinces and their associated glacier systems reacted differently to Holocene changes in climate and ocean circulation in the west Greenland region. Asynchronous timing of deglaciation from northern Melville Bay to Jakobshavn Isbrae, Disko Bay (see Fig.1 for location), has indeed been inferred from $^{14}C$ of $^{10}Be$ dates in lake sediments and moraine deposits, and was partly attributed to peculiarities in the topography of local glacier outlets in this region (Young and Briner, 2015). This last factor has thus to be considered together with regional changes in atmospheric temperature and oceanic circulation when interpreting our XRF-derived dataset.

5.1 The Early Holocene deglaciation of the NW GIS

Numerical models (Lecavalier et al., 2014) as well as $^{14}C$ and $^{10}Be$ dating (Bennike, 2008; Fredskild, 1985; Weidick, 1978) indicate that the deglaciation of the Melville Bay sector of the ice sheet to its historical ice limit was completed between 9.9 and 9.1 cal. kyrs BP, that is up to 2000 years earlier than in central western Greenland. According to Briner et al. (2013) this early ice retreat can be explained by the existence of a marine-based ice sheet along most of Melville Bay which is therefore susceptible to rapid retreat *via* calving.

The continuous vast stretch of marine terminating ice in Melville Bay drains a large part of the NW GIS. Holocene thinning of this sector of the GIS is therefore likely to induce major changes in ice flow and mass balance of Melville Bay glaciers and thus in the delivery of lithic material to the shelf from their marine outlets. We consider that the 9-7.5 cal. kyrs BP interval of maximum relative contribution of Karrat North-derived material to the lithic sedimentation at core 204 CQ is an expression of the early Holocene thinning of the NW GIS as depicted from the nearby Camp Century ice-core (Vinther et al., 2009). The updated calculation of elevation changes at Camp

Century (Lecavalier et al., 2017) suggests that this sector of the GIS experienced the most dramatic episode of thinning of the last 9000 years from ca. 9 to 7.5 cal. kyrs BP (Fig. 6) during the Holocene peak in solar insolation (Berger, 1978). Rates of elevation change throughout this period increased from ca. 2 m/20 years close to 9 cal. kyrs BP to > 4 m/20 years around 7.5 cal. kyrs BP before dropping to a 6 cal. kyrs BP standstill at an elevation slightly lower than the present ice-core altitude (Fig. 6; Lecavalier et al., 2017). Subsequent middle and late Holocene periods of NW GIS thinning ca. 5.5 to 4 cal. kyrs BP, and 2.5 to 1 cal. kyrs BP, occurred in phase with increasing (albeit moderate) relative contribution of Karrat North-derived material to sediments of core 204 CQ (Fig. 6), hence suggesting that even subtle millennial-scale evolution of the NW GIS have implication on the origin of lithic sediments delivered to the nearby shelf.

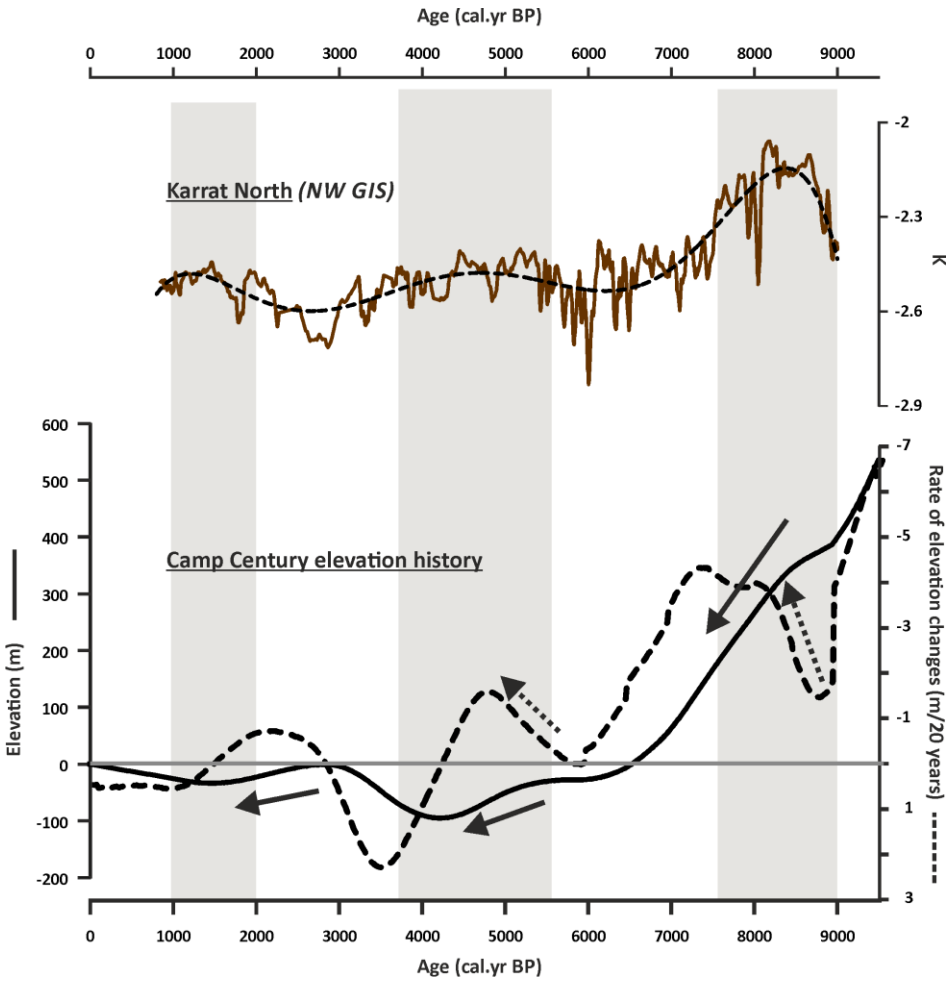

Figure 6: Downcore pattern of the normalized XRF-derived K counts, the elemental marker for Karrat-North (NW GIS)-derived sediment (top), and elevation history of Camp Century, NW GIS, after Lecavalier et al. (2017) (bottom). Elevation expressed according to the modern altitude (horizontal line crossing 0 on the left axis); negative (positive) rates of elevation change on the right axis corresponds to ice thinning (thickening); plain and dotted arrows point to remarkable periods of elevation decrease and increase rates of thinning, respectively.

Finally, in addition to the exceptionally high input of terrigenous material from the NW GIS to the shelf of Melville Bay between ca. 9 and 7.5 cal. kyrs BP (Fig. 5 and 6) which diluted the material sourced from southern sectors of the studied area, other factors might explain the low relative contribution of Upernavik Isstrom-, coastal basaltic- and Rink Isbrae-derived material to sediments of core 204 CQ during this time period: an early Holocene low in WGC flow strength (Perner et al., 2012) reduced the northward transport of southern source lithics; also, high duration of seasonal sea ice off western Greenland until ca. 7.5 cal kyrs BP (Ouellet-Bernier et al., 2014) limited the delivery of calved lithic-laden icebergs from marine terminating glaciers to the nearby marine environment (Fig. 7). The very fine grain size of the lithic material feeding the inner sector of the Upernavik Trough, where core 204 CQ is located, during the early Holocene (Fig. 4) suggests that sedimentation from turbid plumes delivered from the proximal Melville Bay sector of the GIS was the main sedimentary processes at play in this area prior to ca. 7.5 cal kyrs BP. Other studies indicate that large-scale melt water discharges from turbid plumes also characterized more southerly sectors of the western GIS such as the Disko Bay region until around 7.5 cal. kyrs BP (Seidenkrantz et al., 2013).

### 5.2 The Holocene Thermal Maximum in western Greenland: response of lithic sedimentation to higher WGC flow strength and summer atmospheric temperatures

A broad maximum in relative contribution of Upernavik Isstrom and Rink Isbrae-derived material characterizes the 7.5 to 5.5 cal. kyrs BP interval. This time period is part of the so-called Holocene Thermal Maximum (HTM) in Greenland (8-5 cal. kyrs BP) when borehole temperatures from the

GRIP ice core suggest constantly higher values than today (Dahl-Jensen et al., 1998). Threshold lake records indicate that the ice sheet over vast stretches of southwestern Greenland retreated behind its present day extent between 7 and 4 cal. kyrs BP (Larsen et al., 2015; and references therein), if not as early as 6.5 cal. kyrs BP near Jakobshavn Isbrae, Disko Bay (Håkansson et al., 2014). Published $^{10}$Be ages show that while the retreating GIS reached its present limit by 10 cal. kyrs BP in the sector of Upernavik Isstrom and 5.2 cal. kyrs BP at Rink Isbrae, the ice sheet in the regions of Melville Bay, Uummannaq Bay, and Disko Bay continued to retreat behind the present limit until 5-3 cal. kyrs BP (Young and Briner, 2015).

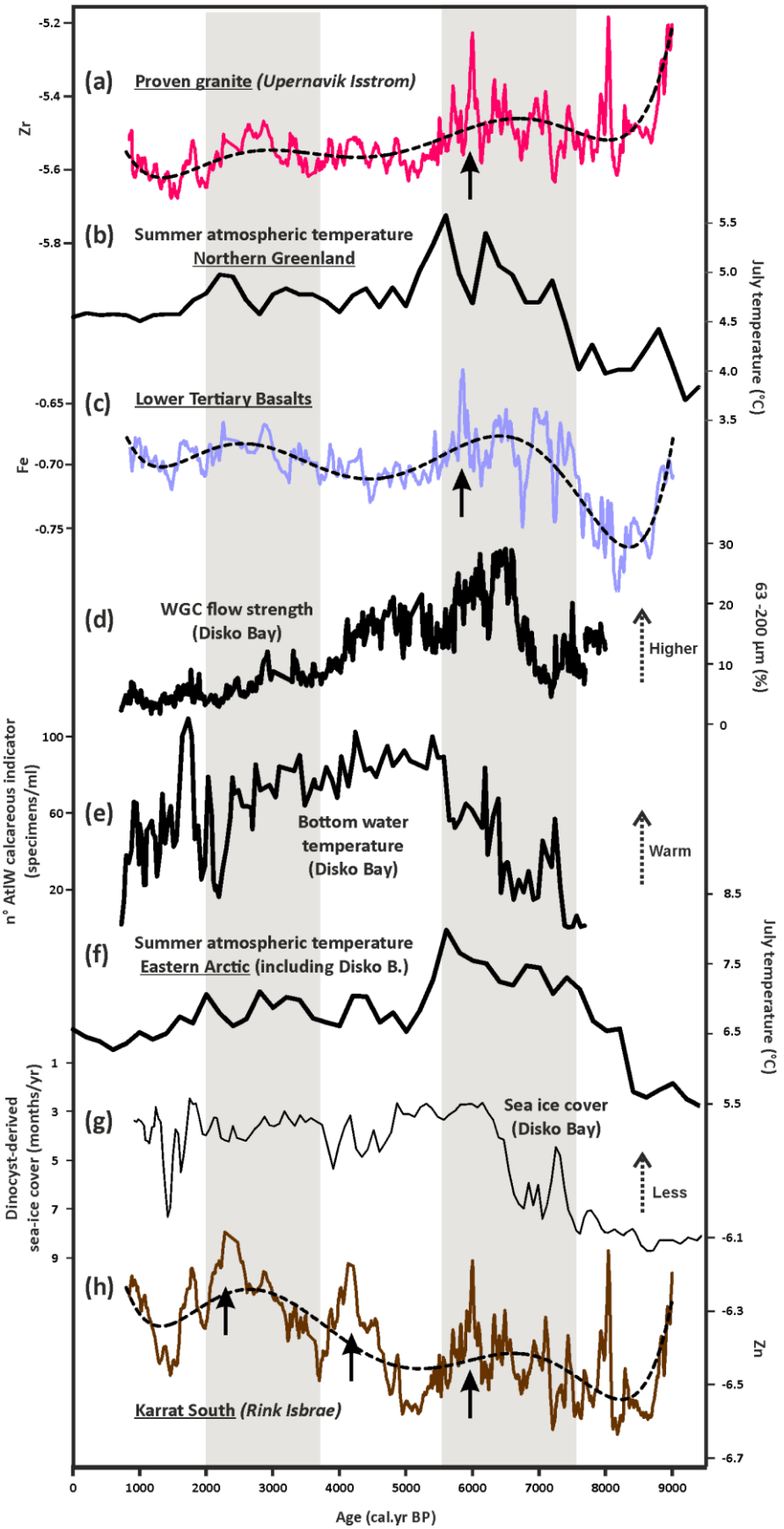
(a) Proven granite (Upernavik Isstrom)
Zr
-5.2
-5.4
-5.6
(b) Summer atmospheric temperature Northern Greenland
-5.8
5.5
5.0
4.5
4.0
3.5
July temperature (°C)
(c) Lower Tertiary Basalts
Fe
-0.65
-0.70
-0.75
(d) WGC flow strength (Disko Bay)
Higher
30
20
10
0
63 -200 µm (%)
n° AtIW calcareous indicator (specimens/ml)
100
60
20
(e) Bottom water temperature (Disko Bay)
Warm
(f) Summer atmospheric temperature Eastern Arctic (including Disko B.)
8.5
7.5
6.5
5.5
July temperature (°C)
Dinocyst-derived sea-ice cover (months/yr)
1
3
5
7
9
(g) Sea ice cover (Disko Bay)
Less
(h) Karrat South (Rink Isbrae)
-6.1
-6.3
-6.5
-6.7
Zn
0
1000
2000
3000
4000
5000
6000
7000
8000
9000
Age (cal.yr BP)

459

Figure 7: Patterns (10 point moving average) of XRF core scanner-derived Zr (a), Fe (c) and Zn (h) relative abundances in core 204 CQ, compared with proxy records of climate and ocean circulation changes. (b): Pollen-derived summer (July) atmospheric temperatures in coastal Northern Greenland (Gajewski et al., 2015). (d): Abundance of fine sand in core 343300, Disko Bay, as an indicator of WGC flow strength (Perner et al., 2013). (e): Abundance of calcareous Atlantic water benthic foraminifera in core 343300, Disko Bay, as indicators of warm WGC (Perner et al., 2013). (f): Pollen-derived summer (July) atmospheric temperatures in Eastern Arctic (Gajewski et al., 2015). (g) Dinocyst-derived sea ice cover in core 343300, Disko Bay (Ouellet-Bernier et al., 2014). The vertical black arrows refer to remarkable events discussed in the text.

There is little evidence that sustained extensive delivery of ice sheet-derived material to the outer WGS occurred after 7.5 cal. kyrs BP (Jennings et al., 2014). This, as well as the HTM trend of decreasing extent of the GIS toward a 5-3 cal. kyrs BP minimum (Young and Briner, 2015; Briner et al., 2016), suggests that most lithic material delivered from marine terminating glaciers during this time period was trapped in the inner part of the WGS. Various Holocene reconstructions show that this GIS expression of the HTM originated as a response to major changes in climate and ocean conditions ca. 7500 years ago, those conditions persisting for several thousand years before Neoglacial cooling. Sedimentological and micropaleontogical proxy archives from the shelf and slope off Disko Bay record a combined strengthening and warming of the WGC from ca. 7.5 to 4 cal. kyrs BP (Perner et al., 2013; Jennings et al., 2014; and Fig. 7). This strengthened WGC was accompanied by reduced sea ice cover (Ouellet-Bernier et al., 2014; and Fig. 7) as a result of both ocean warming and reduced input of melt water following the early Holocene period of major melting and retreat of the GIS. A synthesis of pollen-inferred summer atmospheric temperature reconstructions clearly highlights this interval as the warmest over the last 10 000 years in coastal settings of North and West Greenland, with positive temperature anomalies relative to the long term average ranging from 1 to 2 °C (Gajewski et al., 2015; and Fig. 7).

We consider that our elemental HTM record of high relative contributions of Upernavik Isstrom-, Tertiary basalts-, and Rink Isbrae-derived material to core 204 CQ might, at least partly, explain the observed higher sedimentation rates recorded at the core location during this time period (Fig.

3). Such high sedimentation rates were promoted by the combination of (1) an efficient WGC transport of southern source material to the core location, and (2) a sustained delivery of lithic material from the narrow, deeply-incised Upernavik Isstrom and Rink Isbrae whose marine termini interacted with warm Atlantic Water carried by the WGC. Increased winter precipitation during the HTM in western Greenland as documented by Thomas et al. (2016), might have offset the retreat of these glaciers, preventing them to become land-based despite high glacial velocities and calving rates (Levy et al., 2018).

The high resolution XRF records in core 204 CQ shown here are characterized by a pervasive ~500 year periodicity in peaks and troughs throughout the HTM, suggesting that either or both the delivery of lithic material to the WGS, and the WGC strength, were subjected to high amplitude changes. To our knowledge, no other climatic or oceanic proxy records in the studied area illustrate such an HTM variability. Some of our highest and lowest elemental values ca. 6 cal. kyrs BP are synchronous with a terrestrial and oceanic event recognized in a sediment core of Disko Bay as the most extensive meltwater pulse of the last 8000 years in this region (Moros et al., 2016). This event is near synchronous with the establishment of the modern-like circulation pattern of the WGC in Disko Bay induced by the opening of Vaigat Strait (see Fig. 1 for location; Perner et al., 2013). This opening resulted in the delivery of basaltic material from Disko Island and the Nuussuaq Peninsula to the outer shelf northwest of Disko Bay where it became available to northward transport *via* the main branch of the WGC. We believe that the recorded peak relative contribution of Rink-Isbrae and Upernavik Isstrom lithic material in the sediment of core 204 CQ (Fig. 7) relates to high melt rates of marine terminating glaciers in western Greenland as initially described by Moros et al. (2016) at ca. 6 cal. kyrs BP in Disko Bay. We also interpret the later peak in the delivery of Fe-rich sediment to core 204 CQ at 5.8 cal. kyrs BP (Fig. 7) as reflecting

the opening of the Vaigat Strait and the subsequent northward transport of this excess amount of basaltic material from outer Disko Bay to the Upernavik Trough.

### 5.3 Neoglacial record of Rink Isbrae-derived lithic sedimentation in Upernavik Trough

The transition from the HTM to the Neoglacial period in western Greenland is widely documented as a major shift in oceanic circulation and climate dated ca. 5 cal. kyrs BP, which triggered glacier advances over a wide sector of the western GIS, following minimum ice extent (Larsen et al., 2017). Reconstructions of atmospheric temperatures from coastal lakes in northwestern and western Greenland point to a rapid decrease in July temperatures of up to 2°C over ca. 100 years (Fig. 7 and 8; Gajewski et al., 2015). Following an abrupt negative shift around 5 cal. kyrs BP, winter precipitation thereafter briefly returned to HTM values before progressively decreasing to an overall Holocene low at 2 cal. kyrs BP (Thomas et al., 2016). Oceanic circulation during this cold and arid Neoglacial period over western Greenland was characterized by reduced WGC strength (Perner et al., 2013) compared to the HTM situation. However, relatively high -but fluctuating- contributions of warm Atlantic water influenced both bottom and surface waters until a maximum cooling during the Little Ice Age (Moros et al., 2006 and 2016).

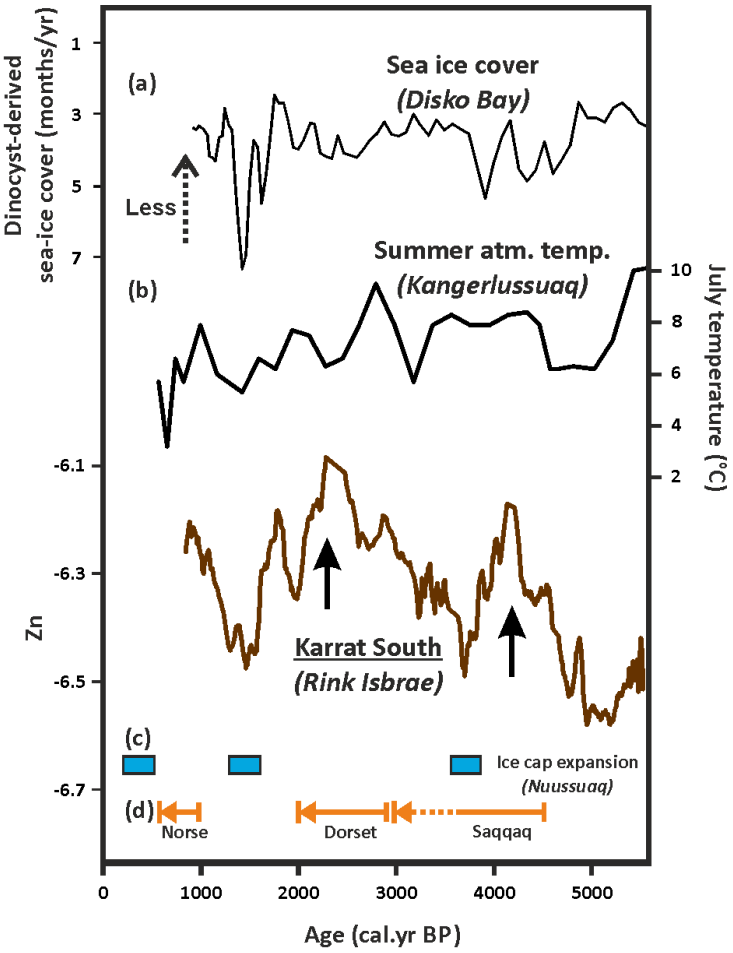


527

528 Figure 8: Post 5.5 cal. kyrs BP changes in relative contribution of Karrat South (Rink Isbrae)-derived material to core
529 204 CQ compared with (a) dinocyst-inferred sea ice cover in Disko Bay, core 343300 (Ouellet-Bernier et al., 2014),
530 (b) pollen-derived summer (July) atmospheric temperatures from Lake 3, Kangerlussuaq sector of western Greenland,
531 150 km south of Disko Bay (Gajewski et al., 2015), (c) the main phases of ice sheet expansion in the Nuussuaq
532 peninsula, southern Uummannaq region (se Fig. 1 for locations), from radiocarbon dating of in-situ moss
533 (Schweinsberg et al., 2017). The vertical plain black arrows refer to remarkable events discussed in the text.
534

535 Our elemental records of lithic sedimentation at core 204 CQ are indicative of a reduced
536 contribution of material derived from the proximal northern Melville Bay ice sheet and Upernavik
537 Isstrom (Fig. 6 and 7) to Upernavik Trough after 5.5 cal. kyrs BP. We interpret this pattern as a
538 rapid response of this northern sector of the western GIS to the inception of Neoglacial cooling in
539 the form of reduced flow rates and possibly stillstand or readvance of the ice margin. This change
540 in glacier dynamics affected both deeply incised fjord areas such as Upernavik Isstrom, and wide
541 marine glacier termini distributed along Melville Bay. A reduced Neoglacial strength of the WGC

as shown by Perner et al. (2012) from Disko Bay proxy records and by our record of basalt-related Fe concentrations in Upernavik Trough (Fig. 7c), likely associated to a progressive southward shift in sea ice cover along western Greenland, were additional factors presumably promoting the lower input of lithic material from proximal, northern tidewater glaciers. Although most model reconstructions and observations agree on a general GIS readvance throughout the Neoglacial from ca. 4 cal. kyrs BP under declining northern hemisphere summer insolation (Lecavalier et al., 2014), our elemental record related to Rink Isbrae-derived material (Fig. 8) suggests that this glacier was an effective sediment supplier to the WGS and core 204 CQ over the last 5000 years, with relative contributions often higher than those recorded during the HTM. Part of this pattern, especially the long term highs in relative concentrations of Rink Isbrae-derived sediments, is obviously induced by the synchronous long term lows in concentrations of material delivered by Melville Bay glaciers and Upernavik Isstrom. However, a reduced WGC strength during the Neoglacial period (Fig. 7, and Perner et al., 2012) suggests that sediment supply by Rink Isbrae to the WGS was particularly enhanced during the Late Holocene despite generally unfavorable climate and ocean conditions over western Greenland. Part of this paradox might lay in the peculiar geomorphology of the Rink Isbrae fjord: according to Chauché et al. (2014), the deep fjord basin hosting the glacier implies that a large proportion of its submerged front is exposed to warm Atlantic waters, resulting in homogeneous, widespread calving and submarine melting across the entire front of this glacier. The sedimentation of Rink-Isbrae material to core 204 CQ (Fig. 8) strongly oscillates at a millennial pace, suggesting that changes in climatic and/or oceanic conditions influenced fluctuations in glacier mass balance. Major events of snowline depression and glacier advance in the Nuussuaq Peninsula, southern Uummannaq Bay, and in southwest Greenland ca. 3.7 cal. kyrs BP and 1.5 cal. kyrs BP have been inferred by Schweinsberg et al. (2017, 2018) from $^{14}C$ dating

of recently ice-entombed moss and the analysis of pro-glacial lake sediment. Interestingly, these two events correspond to periods of reduced delivery of Rink Isbrae material to core 204 CQ (Fig. 8). Accompanying proxy records of sea ice cover in Disko Bay (Ouellet-Berniet et al., 2014), of summer atmospheric temperatures in the Kangerlusssuaq region (Gajewski et al., 2015), suggest that these glacier advances were broadly linked to colder oceanic and atmospheric conditions (Fig. 8). Our XRF-derived high resolution record of Rink-Isbrae dynamics therefore holds a less local significance than initially expected, and might well illustrate the evolution of the climate of western Greenland during the Neoglacial.

## 6 Conclusions

The high resolution geochemical (elemental) proxy records presented in this study reveal major changes in the provenance of lithogenic material in the Upernavik Trough, northern sector of the WGS, over the last 9100 years. Our records reflect the distinct dynamics of the main proximal and distal (southern) marine terminating glaciers of Western Greenland as well as changes in the efficiency of sediment transport and redistribution by the WGC.

Contributions from the proximal Melville Bay glaciers were dominant during the early part of the record up to ca 7.5 cal. kyrs BP. This strong influence of local material was the result of the rapid retreat of a vast stretch of the NW GIS during the most dramatic thinning it experienced over the course of the last 9000 years. Limited Early Holocene contributions from southern source areas (basaltic formations, Upernavik Isstrom and Rink Isbrae) are explained by a combination of low WGC strength and the buttressing effect of high sea-ice concentrations on calving glaciers.

Atmospheric warming, accelerated melting of marine terminating glaciers under strengthened WGC, and reduced sea-ice concentrations from 7.5 cal. kyrs BP onwards triggered the increasing

588 contributions of distal southern sources to the lithic sedimentation over Upernavik Trough. These
589 contributions, which culminated at ca. 6 cal. kyrs BP, are indicative of sustained high velocities
590 and calving rates of Upernavik Isstrom and Rink Isbrae, under the influence of high winter
591 precipitation over the western GIS during the HTM.
592 The Neoglacial shift in atmospheric and oceanic circulation ca. 5 cal. kyrs BP led to a general
593 reduction in the delivery of lithic material from outlet glaciers of the western GIS to the WGS. The
594 peculiar geomorphology of the (deep) fjord hosting Rink Isbrae, combined with the (great) depth
595 of the cross-shelf Uummannaq Trough likely explain the sensitivity of Rink Isbrae to submarine
596 melting and hence the recorded high sediment supply by this glacier despite lower WGC strength.
597 Millennial-scale oscillations in Rink Isbrae-derived sedimentation at the studied core location are
598 indicative of fluctuations in the mass balance of this glacier which occurred in phase with major
599 glacier advances reported elsewhere in West and Southwest Greenland throughout the Neoglacial
600 period.
601 The present study offers a high-resolution framework of the western GIS dynamics and their link
602 with major changes in regional climatic and oceanic circulation throughout the last 9100 years.
603 This reconstruction is likely to provide a practical basis for future investigations testing the impact
604 of summer Greenland blocking events and North-Atlantic sea-surface temperature changes upon
605 the Holocene variability of western GIS melt (Graeter et al., 2018) as well as the wider ocean
606 dynamics linkages between the WGC, the North Atlantic Current and the strength of the Sub-Polar
607 Gyre (Goslin et al., 2018).

## Acknowledgments

This work is a contribution to the GREENEDGE project funded by the French Agence Nationale de la Recherche and the Fondation Total, and coordinated by Marcel Babin (Takuvik, CNRS-University Laval, Canada). We acknowledge additional funding provided by the Initiative d'Excellence (IdEx) programme of the University of Bordeaux and by the Natural Science and Engineering Research Council of Canada (NSERC), as well as support from the Network of Centres of Excellence ArcticNet. Kerstin Perner, Leibniz Institute for Baltic Sea Research, Germany, is thanked for having shared with us selected proxy records from Disko Bay. Finally, we wish to thank the CCGS Amundsen captain, officers and crew for their support during the 2014 ArcticNet cruise.

## References

Alley, R.B., Mayewski, P.A., Sowers, T., Stuiver, M., Taylor, K.C., Clark, P.U., 1997. Holocene climatic instability: a prominent, widespread event 8200 years ago. Geology 25, 483–486.

Andresen, C.S., Kjeldsen, K.K., Harden, B., Nørgaard-Pedersen, N., Kjær, K.H., 2014. Outler glacier dynamics and bathymetry at Upernavik Isstrøm and Upernavik Isfjord, North-West Greenland. Geological Survey of Denmark and Greenland Bulletin 31, 79-82.

Andrews, J.T., Jull, A. J. T., Donahue, D. J., Short, S. K., Osterman, L. E., 1985. Sedimentation rates in Baffin Island fiord cores from comparative radiocarbon dates. Canadian Journal of Earth Sciences, 22: 1827-1934.

Andrews, J.T., & Eberl, D. (2011). Surface (sea floor) and near-surface (box cores) sediment mineralogy in Baffin Bay as a key to sediment provenance and ice sheet variations. Canadian Journal of Earth Sciences, 48: 1307-1328

Andrews, J.T., Barber, D.C., Jennings, A.E., Eberl, D.D., Maclean, B., Kirby, M.E., Stoner, J.S., 2012. Varying sediment sources (Hudson Strait, Cumberland Sound, Baffin Bay) to the NW Labrador Sea slope between and during Heinrich events 0 to 4. Journal of Quaternary Science 27, 475-484.

Andrews, J.T., Klein, A.J., Jenner, K.A., Jennings, A.E., Campbell, C., 2018. The variability of Baffin Bay seafloor sediment mineralogy: the identification of discrete glacial sediment sources and application to Late Quaternary downcore analysis. Canadian Journal of Earth Sciences, 2018, 55(6): 620-639.

Baumann, J., Chaumillon, E., Schneider, J.-L., Jorissen, F., Sauriau, P.-G., Richard, P., Bonnin, J., Schmidt, S., 2017. Contrasting sediment records of marine submersion events related to wave exposure, Southwest France. Sedimentary Geology 353, 158-170.

Bennike, O., 2008. An early Holocene Greenland whale from Melville Bugt, Greenland. Quaternary Research 69, 72-76.

Berger, A., 1978. Long-term variations of daily insolation and Quaternary climate changes. Journal of Atmospheric Sciences 35, 2362-2367.

Blaauw, M., Christen, J.A., 2011. Flexible paleoclimate age-depth models using an autoregressive gamma process. Bayesian Analysis 6, 457-474

Bouchard, F., P. Francus, R. Pienitz, Laurion I., 2011. Sedimentology and geochemistry of thermokarst ponds indiscontinuous permafrost, subarctic Quebec, Canada,J. Geophys. Res. 116, G00M04, doi:10.1029/2011JG001675.

Briner, J.P., Håkansson, L., Bennike, O., 2013. The deglaciation and neoglaciation of Upernavik Isstrom, Greenland. Quaternary Research 80, 459-467.

Briner, J.P., McKay, N.P., Axford, Y., Bennike, O., Bradley, R.S., de Vernal, A., Fisher, D., Francus, P., Fréchette, B., Gajewski, K., Jennings, A., Kaufman, D.S., Miller, G., Rouston, C., Wagner, B., 2016. Quaternary Science Reviews 147, 340-364.

Calvert, S.E., Pedersen, T.F., 2007. Elemental proxies for palaeoclimatic and palaeoceanographic variability in marine sediments: interpretation and application, in: Hillaire-Marcel, C., de Vernal, A. (Eds.), Developments in Marine Geology, Volume 1. Proxies in Late Cenozoic Paleoceanography. Elsevier, New York, pp. 567-644.

Caron, M., St-Onge, G., Montero-Serrano, J.-C., Rochon, A., Georgiadis, E., Giraudeau, J., Massé, G., 2018. Holocene chronostratigraphy of northeastern Baffin Bay based on radiocarbon and palaeomagnetic data. Boreas. https://doi.org/10.1111/bor.12346. ISSN 0300-9483.

Chauché, N., Hubbard, A., Gascard, J.-C., Box, J.E., Bates, R., Koppes, M., Sole, A., Christoffersen, P., Patton, H., 2014. Ice-ocean interaction and calving front morphology at two west Greenland tidewater outlet glaciers. The Cryosphere 8, 1457-1468.

Cuven, S., Francus, P., Lamoureux, S., 2011. Mid to Late Holocene hydroclimatic and geochemical records from the varved sediments of East Lake, Cape Bounty, Canadian High Arctic. Quaternary Science Reviews 30 (19-20), 2651-2665.

Dahl-Jensen, D., Mosegaard, K., Gundestrup, N., Clow, G.D., Johnsen, S.J., Hansen, A.W., Balling, N., 1998. Past temperatures directly from the Greenland ice sheet. Science 282, 268-271.

Escher, J.C., Pulvertaft, T.C.R., 1995. Geological map of Greenland, 1:2 500 000. Copenhagen: Geological Survey of Greenland.

Fillon, R.H., Hardy, I.A., Wagner, F.J.E., Andrews, J.T., Josenhans, H.W., 1981. Labrador Shelf : shell and total organic matter – 14C discrepancies. In Current research, part B. Geological Survey of Canada, Paper 81-1B, pp. 105-111.

Fortin, D., Francus, P., Gebhardt, A. C., Hahn, A., Kliem, P., Lisé-Pronovost, A., 2013. Destructive and non-destructive density determination: method comparison and evaluation from the Laguna Potrok Aike sedimentary record. Quaternary Science Reviews 71, 147–153.

675 Fredskild, B., 1985. The Holocene vegetational development of Tugtuligssuaq and Qeqertat, Northwest Greenland.
676 Meddelelser om Grønland. Geoscience 14 (20 pp.).

677 Gajewski, K., 2015. Quantitative reconstruction of Holocene temperature across the Canadian Arctic and Greenland.
678 Global and Planetary Change 128, 14-23.

679 Goslin, J., Fruergaard, M., Sander, L., Galka, M., Menviel, L., Monkenbusch, J., Thibault, N., Clemmensen, L.B.,
680 2018. Holocene centennial to millenial shifts in North-Atlantic storminess and ocean dynamics. Nature Scientific
681 Reports 8, 12778.

682 Graeter, K.A., Osterberg, E.C., Ferris, D.G., Hawley, R.L., Marshall, H.P., Lewis, G., Meehan, T., McCarthy, F.,
683 Overly, T., Birkel, S.D., 2018. Ice core records of west Greenland melt and climate forcing. Geophysical Research
684 Letters 45, 3164-3172.

685 Håkansson, L., Briner, J.P., Andresen, C.S., Thomas, E.K., Bennike, O., 2014. Slow retreat of a land based sector of
686 the west Greenland ice sheet during the Holocene thermal maximum: evidence from threshold lakes at Paakitsoq.
687 Quaternary Science Reviews 98, 74-83.

688 Henriksen, N., Higgins, A.K., Kalsbeek, F., Pulvertaft, T.C.R., 2000. Greenland from Archaean to Quaternary.
689 Descriptive text to the Geological map of Greenland, 1:2 500 000. Geology of Greenland Survey Bulletin 185.

690 Hogan, K.A., Ó Cofaigh, C., Jennings, A.E., Dowdeswell, J.A., Hiemstra, J.F., 2016. Deglaciation of a major palaeo-
691 ice stream in Disko Trough, West Greenland. Quaternary Science Reviews 147, 5-26.

692 Jennings, A.E., Walton, M.E., Ó Cofaigh, C., Kilfeather, A., Andrews, J.T., Ortiz, J.D., de Vernal, A., Dowdeswell,
693 J.A., 2014. Paleoenvironments during Younger Dryas-Early Holocene retreat of the Greenlnad Ice Sheet from outer
694 Disko Trough, central west Greenland. Jiurnal of Quaternary Science 29(1), 27-40.

695 Jennings, A.E., Andrews, J.T., Ó Cofaigh, C., St Onge, G., Sheldon, C., Belt, S.T., Cabedo-Sanz, P., Hillaire-Marcel,
696 C., 2017. Ocean forcing of Ice Sheet retreat in central west Greenland from LGM to the early Holocene. Earth and
697 Planetary Science Letters 472, 1-13.

698 Jennings, A.E., Andrews, J.T., Ó Cofaigh, C., St-Onge, G., Belt, S., Cabedo-Sanz, P., Pearce, C., Hillaire-Marcel, C.,
699 Campbell, D.C., 2018. Baffin Bay paleoenvironments in the LGM and HS1: Resolving the ice-shelf question. Marine
700 Geology 402, 5-16.

701 Krawczyk, D.W., Witkowski, A., Moros, M., Lloyd, J.M., Hoyer, J.L., Miettinen, A., Kuijpers, A., 2016. Quantitative
702 reconstruction of Holocene sea ice and sea surface temperature off West Greenland from the first regional diatom data
703 set. Paleoceanography 32, 18-40.

704 Larsen, N.K., Kjaer, K.H., Lecavalier, B., Bjork, A., Colding, S., Huybrechts, P., Jakobsen, K.E., Kjeldsen, K.K.,
705 Knudsen, K.-L., Odgaard, B.V., Olsen, J., 2015. The response of the southern Greenland ice sheet to the Holocene
706 thermal maximum. Geology 43 (4), 291-294.

707 Larsen, N.K., Strunk, A., Levy, L.B., Olsen, J., Bjørk, A., Lauridsen, T.L., Jeppesen, E., Davidson, T.A., 2017. Strong
708 altitudinal control on the response of local glaciers to Holocene climate change in southwest Greenland. Quaternary
709 Science Reviews 168, 69-78.

710 Lecavalier, B.S., Milne, G.A., Simpson, M.J.R., Wake, L., Huybrechts, P., Tarasov, L., Kjeldsen, K.K., Funder, S.,
711 Long, A.J., Woodroffe, S., Dyke, A.S., Larsen, N.K., 2014. A model of Greenland ice sheet deglaciaition constrained
712 by observations of relative sea level and ice extent. Quaternary Science Reviews 102, 54-84.

Lecavalier, B.S., Fisher, D.A., Milne, G.A., Vinther, B.M., Tarasov, L., Huybrechts, P., Lacelle, D., Main, B., Zheng, J., Bourgeois, J., Dyke, A.S., 2017. High Arctic Holocene temperature record from the Agassiz ice cap and Greenland ice sheet evolution. PNAS 114(23), 5952-5957.

Levy, L.B., Kelly, M.A., Applegate, P.A., Howley, J.A., Virginia, R.A., 2018. Middle to late Holocene chronology of the western margin of the Greenland Ice Sheet: A comparison with Holocene temperature and precipitation records. Arctic, Antarctic, and Alpine Research, 50:1, DOI: 10.1080/15230430.2017.1414477

Licht, K.J., Cunningham, W.L., Andrews, J.T., Domack, E.W., Jennings, A.E., 1998. Establishing chronologies from acid-insoluble organic 14C dates on antarctic (Ross Sea) and arctic (North Atlantic) marine sediments. Polar Research 17(2), 203-216.

Lloyd, J.M., Park, L.A., Kuijpers, A., Moros, M., 2005. Early Holocene palaeoceanography and deglacial chronology of Disko Bugt, West Greenland. Quaternary Science Reviews 24, 1741-1755.

Lloyd, J.M., Kuijpers, A., Long, A., Moros, M., Park, L.A., 2007. Foraminiferal reconstruction of mid- to late-Holocene ocean circulation and climate variability in Disko Bugt, West Greenland. The Holocene 17(8), 1079-1091.

Lloyd, J., Moros, M., Perner, K., Telford, R.J., Kuijpers, A., Jansen, E., McCarthy, D., 2011. A 100 yr record of ocean temperature control on the stability of Jakobshavn Isbrae, West Greenland. Geology 39 (9), 867–870.

MacGregor, J.A., Colgan, W.T., Fahnestock, M.A., Morlighem, M., Catania, G.A., Paden, J.D., Goginemi, S.P., 2016. Holocene deceleration of the Greenland Ice Sheet. Science 351 (6273), 590-593.

Martin, L., Mooney, S., Goff, J., 2014. Coastal wetlands reveal a non-synchronous island response to sea-level change and a palaeostorm record from 5.5 kyr to present. The Holocene 24(5), 569–580.

Meyers, P.A., 1994. Preservation of elemental and isotopic source identification of sedimentary organic matter. Chemical Geology 114, 289-302.

Moros, M., Jensen, K.G., Kuijpers, A., 2006. Mid- to late-Holocene hydrological and climatic variability in Disko Bugt, central West Greenland. The Holocene 16(3), 357-367.

Moros, M., Lloyd, J.M., Perner, K., Krawczyk, D., Blanz, T., de Vernal, A., Ouellet-Bernier, M.-M., Kuijpers, A., Jennings, A.E., Witkowski, A., Schneider, R., Jansen, E., 2016. Surface and sub-surface multi-proxy reconstruction of middle to late Holocene palaeoceanographic changes in Disko Bugt, West Greenland. Quaternary Science Reviews 132, 146-160.

Myers, P.G., Kulan, N., Ribergaard, N.H., 2007. Irminger Water variability in the West Greenland Current. Geophysical Research Letters 34, L17601.

Newton, A.M.W., Knutz, P.C., Huuse, M., Gannon, P., Brocklehurst, S.H., Clausen, O.R., Gong, Y., 2017. Ice stream reorganization and glacial retreat on the northwest Greenland shelf. Geophysical Research Letters 44, doi:10.1002/2017GL073690.

Ó Cofaigh, C., Dowdeswell, J.A., 2001. Laminated sediments in glacimarine environments: diagnostic criteria for their interpretation. Quaternary Science Reviews 20, 1411-1436.

Ó Cofaigh, C., Dowdeswell, J.A., Jennings, A.E., Hogan, K.A., Kilfeather, A., Hiemstra, J.F., Noormets, R., Evans, J., McCarthy, D.J., Andrews, J.T., Lloyd, J.M., Moros, M., 2012. An extensive and dynamic ice sheet on the West Greenland shelf during the last glacial cycle. Geology 41(2), 219-222.

751 Ouellet-Bernier, M.-M., de Vernal, A., Hillaire-Marcel, C., Moros, M., 2014. Paleoceanographic changes in the Disko
752 Bugt area, West Greenland, during the Holocene. The Holocene 24(11), 1573-1583.

753 Perner, K., Moros, M., Jennings, A., Lloyd, J.M., Knudsen, K.L., 2012. Holocene palaeoceanographic evolution off
754 West Greenland. The Holocene 23(3), 374-387.

755 Perner, K., Moros, M., Snowball, I., Lloyd, J.M., Kuijpers, A., Richter, T., 2013. Establishment of modern circulation
756 pattern at c. 6000 cal a BP in Disko Bugt, central West Greenland: opening of the Vaigat Strait. Journal of Quaternary
757 Science 28(5), 480-489.

758 Rignot, E., Mouginot, J., 2012. Ice flow in Greenland for the International Polar Year 2008-2009. Geophysical
759 Research Letters 39, L11501.

760 Sakakibara, D., Sugiyama, S., 2018. Ice front and flow speed variations of marine-terminating outlet glaciers along
761 the coast of Prudhoe Land, northwestern Greenland. Journal of Glaciology 64(244), 300-310.

762 Schweinsberg, A.D., Briner, J.P., Miller, G.H., Bennike, O., Thomas, E.K., 2017. Local glaciation in West Greenland
763 linked to North Atlantic Ocean circulation during the Holocene. Geology 45(3), 195-198.

764 Schweinsberg, A.D., Briner, J.P., Miller, G.H., Lifton, N.A., Bennike, O., Graham, B.L., 2018. Holocene mountain
765 glacier history in the Sukkertoppen Iskappe area, southwest Greenland. Quaternary Science Reviews, 197, 142-161.

766 Seidenkrantz, M.-S., Ebbesen, H., Aagaard-Sørensen, S., Moros, M., Loyd, J.M., Olsen, J., Knudsen, M.F., Kuijpers,
767 A., 2013. Early Holocene large-scale meltwater discharge from Greenland documented by foraminifera and sediment
768 parameters. Palaeogeography, Palaeoclimatology, Palaeoecology 391 (A), 71-81.

769 Sha, L., Jiang, H., Seidenkrantz, M.-S., Knudsen, K.L., Olsen, J., Kuijpers, A., Liu, Y., 2014. A diatom-based sea-ice
770 reconstruction for the Vaigat Strait (Disko Bugt, West Greenland) over the last 5000 yr. Palaeogeography,
771 Palaeoclimatology, Palaeoecology 403, 66-79.

772 Sheldon, C., Jennings, A., Andrews, J.T., Ó Cofaigh, C., Hogan, K., Dowdeswell, J.A., Seidenkrantz, M.-S., 2016.
773 Ice stream retreat following the LGM and onset of the west Greenland current in Uummannaq Trough, west Greenland.
774 Quaternary Science Reviews 147, 27-46.

775 Simon, Q., Hillaire-Marcel, C., St-Onge, G., Andrews, J.T., 2013. North-eastern Laurentide, western Greenland and
776 southern Innuitian ice stream dynamics during the lastglacial cycle. Journal of Quaternary Science 29(1), 14-26.

777 Sinclair, G., Carlson, A.E., Mix, A.C., Lecavalier, B.S., Milne, G., Mathias, A., Buizert, C., DeConto, R., 2016.
778 Diachronous retreat of the Greenland ice sheet during the last deglaciation. Quaternary Science Reviews 143, 243-
779 258.

780 Steenfelt, A., Thomassen, B., Lind, M., Kyed, J., 1998. Karrat 97: reconnaissance mineral exploration in central West
781 Greenland. Geology of Greenland Survey Bulletin 180, 73-80.

782 Steenfelt, A., 2001. Geochemical atlas of Greenland – West and South Greenland. Danmarks og Grønlands Geologiske
783 Undersøgelse Rapport 2001/46, 39 pp.

784 Stern, H.L., Heide-Jørgensen, M.P., 2003. Variability of sea ice in Baffin Bay and Davis Strait. Polar Research 22(1),
785 11-18.

786 Stuiver, M., Reimer, P.J., Reimer, R.W., 2018. CALIB 7.1 [WWW program] at http://calib.org

Thomas, E.K., Briner, J.P., Ryan-Henry, J.J., Huang, Y., 2016. A major increase in wionter snowfall during the middle Holocene on western Greenland caused by reduced sea ice in Baffin Bay and the Labrador Sea. Geophysical Research Letters 43, 5302-5308.

Vinther, B., Buchardt, S.L., Clausen, H.B., Dahl-Jensen, D., Johnsen, S.J., Fisher, D.A., Koerner, R.M., Raynaud, D., Lipenkov, V., Andersen, K.K., Blunier, T., Rasmussen, S.O., Steffensen, J.P., Svensson, A.M., 2009. Holocene thinning of the Greenland ice sheet. Nature 461, 385-388.

Wang, J., Mysak, L.A., Ingram, R.G., 1994. Interannual variabilityof sea-ice cover in Hudson Bay, Baffin Bay and the Labrador Sea, Atmosphere-Ocean 32(2), 421-447.

Weidick, A., 1958. Frontal variations at Upernaviks Isstrøm in the last 100 years. Meddelelser fra Dansk Geologisk Forening 14, 52-60.

Weidick, A., 1978. $^{14}$C dating of survey material carried out in 1977. Rapport Grønlands Geologiske Undersøgelse 90, 119-124.

Weltje, G.J., Tjallingii, R., 2008. Calibration of XRF core scanners for quantitative geochemical logging of sediment cores: theory and application. Earth and Planetary Science Letters 274, 423-438.

Young, N.E., Briner, J.P., Stewart, H.A.M., Axford, Y., Csatho, B., Rood, D.H., Finkel, R.C., 2011. Response of Jakobshavn Isbrae, Greenland, to Holocene climate. Geology 39(2), 131-134.

Young, N.E., Briner, J.P., 2015. Holocene evolution of the western Greenland Ice Sheet: Assessing geophysical ice-sheet models with geological reconstructions of ice-margin change. Quaternery Science Reviews 114, 1-17.

Appendix for

# A high-resolution elemental record of post-glacial lithic sedimentation in Upernavik Trough, western Greenland: history of ice-sheet dynamics and ocean circulation changes over the last 9 100 years

J. Giraudeau[1], E. Georgiadis[1,2], M. Caron[3], P. Martinez[1], G. Saint-Onge[3], I. Billy[1], P. Lebleu[1], and O. Ther[1], and G. Massé[2,4]

[1]Université de Bordeaux, CNRS, UMR 5805 EPOC, 33615 Pessac, France

[2]Université Laval, CNRS, UMI 3376 TAKUVIK, Québec, G1V 0A6, Canada

[3]Université du Québec à Rimouski and GEOTOP Research Center, Institut des sciences de la mer de Rimouski (ISMER), Rimouski, G5L 3 A1, Canada

[4]Université Paris VI, CNRS, UMR 7159 LOCEAN, 75005 Paris, France

**Contents of this file**

Figures S1, Table S1

**Introduction**

The supplementary figure (Fig. S1) provides additional constraints to the construction of the age-depth model of core 204 CQ.

The supplementary table (Tab. S1) provides results of the Linear Discriminant Analysis (LDA) applied on ranges of element and oxide concentrations within each of the main geological provinces of western Greenland from 75°N to 68°N according to the geochemical database compiled by Steenfelt (2001). These results are plotted within the main text as Fig. 2.

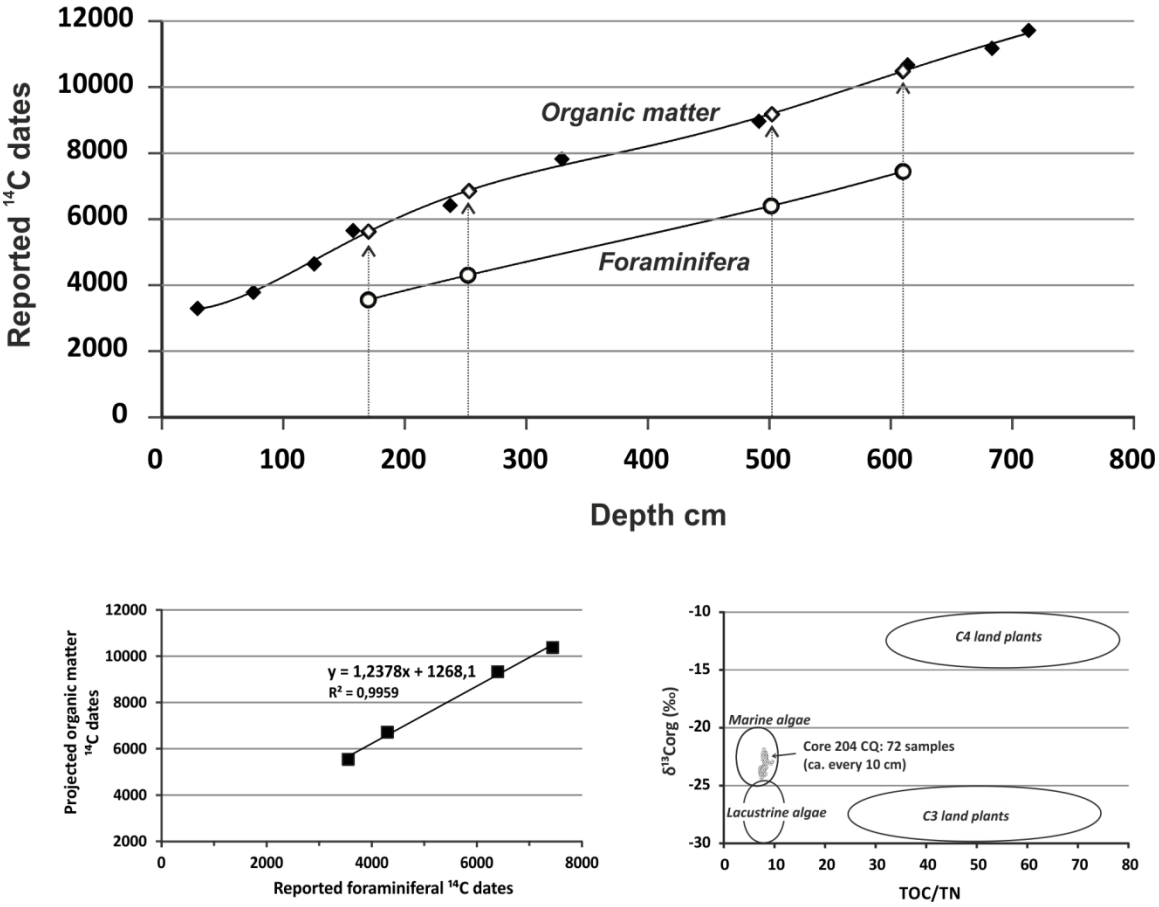


**Figure S1.** Top: Reported (uncorrected, uncalibrated) $^{14}C$ dates obtained on foraminiferal (empty circles) and organic matter (full diamonds) samples. Projected organic matter $^{14}C$ dates (empty diamonds) at the core depth of foraminiferal $^{14}C$ dates according to their intercept with a $4^{th}$ order polynomial fit of the whole set of $^{14}C$ dates measured on organic matter. Bottom left: plot of projected organic matter $^{14}C$ dates vs. foraminiferal $^{14}C$ dates and linear equation [1] used to correct for ageing by reworked "old" carbon all reported $^{14}C$ dates measured on organic matter. Bottom right: elemental and isotopic identifiers of source organic matter (after Meyers, 1994) and plot of C/N ratios and organic $d^{13}C$-values measured in core 204 CQ.

***Linear discriminant analyses (LDAs)***

| ***Oxides (%)*** | | | ***Elements (ppm)*** | | |
|---|---|---|---|---|---|
| **Axis** | **Eigenvalues** | **Percent** | **Axis** | **Eigenvalues** | **Percent** |
| 1 | 164.55 | 98.04 | 1 | 11.14 | 62.09 |
| 2 | 2.59 | 1.54 | 2 | 5.37 | 29.94 |
| | | | | | |
| **Loadings** | **Axis 1** | **Axis 2** | **Loadings** | **Axis 1** | **Axis 2** |
| **Al2O3** | 0.29 | -0.53 | **Cr** | -62.20 | -192.52 |
| **TiO2** | -0.10 | 0.19 | **Ni** | -32.22 | -72.60 |
| **Fe2O3** | -0.38 | 0.78 | **Rb** | 17.27 | 10.00 |
| **K2O** | 0.11 | 0.34 | **Zn** | 12.50 | -47.08 |
| | | | **Zr** | 67.22 | 190.07 |
| | | | | | |
| **Scores (range)** | **Axis 1** | **Axis 2** | **Scores (range)** | **Axis 1** | **Axis 2** |
| **Karrat North** | 7.14 to 7.06 | 0.15 to -0.77 | **Karrat North** | 2.54 to 3.31 | -0.35 to -0.63 |
| **Proven Granite** | 6,09 to 6.75 | 0,93 to 2,92 | **Proven Granite** | 1.66 to 0.09 | 1.38 to 3.66 |
| **Tertiary basalts** | -17.55 to -17.39 | 0.75 to -0.28 | **Tertiary basalts** | -3.43 to -4.62 | -0.58 to -0.82 |
| **Karrat South** | 1.38 to -1.04 | -1.02 to 0.51 | **Karrat South** | 1.00 to 1.32 | -1.63 to -2.98 |
| **Archean gneiss** | 2.82 to 4.72 | -2.26 to -0.93 | **Archean gneiss** | -2.11 to 0.21 | 0.13 to 1.82 |

**Table S1.** Results of the Linear Discriminant Analyses (LDAs) applied on ranges of element and oxide concentrations within each of the main geological provinces of western Greenland from 75°N to 68°N according to the geochemical database compiled by Steenfelt (2001). These results are plotted within the main text as Fig. 2.